© 2021. Published by The Company of Biologists Ltd | Development (2021) 148, dev199425. doi:10.1242/dev.199425

RESEARCH ARTICLE

Cell wall damage attenuates root hair patterning and tissue morphogenesis mediated by the receptor kinase STRUBBELIG

Ajeet Chaudhary[1,*], Xia Chen[1], Barbara Leśniewska[1], Rodion Boikine[1], Jin Gao[1,‡], Sebastian Wolf[2] and Kay Schneitz[1,§]

ABSTRACT

Cell wall remodeling is essential for the control of growth and development as well as the regulation of stress responses. However, the underlying cell wall monitoring mechanisms remain poorly understood. Regulation of root hair fate and flower development in *Arabidopsis thaliana* requires signaling mediated by the atypical receptor kinase STRUBBELIG (SUB). Furthermore, SUB is involved in cell wall integrity signaling and regulates the cellular response to reduced levels of cellulose, a central component of the cell wall. Here, we show that continuous exposure to sub-lethal doses of the cellulose biosynthesis inhibitor isoxaben results in altered root hair patterning and floral morphogenesis. Genetically impairing cellulose biosynthesis also results in root hair patterning defects. We further show that isoxaben exerts its developmental effects through the attenuation of SUB signaling. Our evidence indicates that downregulation of SUB is a multi-step process and involves changes in SUB complex architecture at the plasma membrane, enhanced removal of SUB from the cell surface, and downregulation of *SUB* transcript levels. The results provide molecular insight into how the cell wall regulates cell fate and tissue morphogenesis.

KEY WORDS: *Arabidopsis*, Cellulose, Cell wall, Cell wall signaling, Isoxaben, Receptor kinase

INTRODUCTION

Plant cells are encapsulated by a semi-rigid cell wall. As a consequence, cell wall remodeling represents a central pillar in the control of growth, development and the defense against abiotic and biotic stresses. In recent years, the mechanisms monitoring and modulating cell wall integrity in plants have received much attention (Bacete et al., 2018; Gigli-Bisceglia et al., 2020; Rui and Dinneny, 2020). However, the molecular framework controlling signaling from the cell wall during development and stress responses is still poorly understood.

The plant cell wall is composed of carbohydrates, including cellulose, hemicellulose, pectin and phenolic compounds, but also contains a large number of cell-wall-bound proteins (Höfte and Voxeur, 2017; Lampugnani et al., 2018). Cellulose synthesis is carried out by cellulose synthase (CESA) protein complexes (CSCs) at the plasma membrane. The CESA1, CESA3 and CESA6 subunits represent the core CSC subunits of the primary cell wall of expanding cells (Desprez et al., 2007; Persson et al., 2007). The herbicide isoxaben induces a rapid clearing of CESA complexes from the plasma membrane (Paredez et al., 2006). The reaction to cellulose biosynthesis inhibition (CBI) induced by isoxaben or by defects in CESA subunits represents a well-characterized compensatory cell wall damage (CWD) response (Gigli-Bisceglia et al., 2020; Vaahtera et al., 2019). Factors implicated as cell wall sensors mediating this response include the cell surface receptor kinase THESEUS 1 (THE1) (Hématy et al., 2007), a member of the *Catharanthus roseus* RECEPTOR-LIKE KINASE 1-LIKE (CrRLK1L) subfamily, and the leucine-rich repeat (LRR) receptor kinase MIK2 (LRR-KISS) (Van der Does et al., 2017), among others (Rui and Dinneny, 2020).

The role of the cell wall in morphogenesis has long been appreciated. Cell wall remodeling is central to cellular growth (Cosgrove, 2018). In addition, the cell wall tightly connects neighboring cells. There is growing evidence that differential growth in physically coupled cells causes mechanical stresses that may in turn influence morphogenesis (Echevin et al., 2019; Uyttewaal et al., 2012; Whitewoods and Coen, 2017). Interestingly, the extracellular matrix of animal cells as well as the cellulose-containing cell wall of brown algae have been shown to influence cell fate (Berger et al., 1994; Hynes, 2009; Watt and Fujiwara, 2011), but a clear demonstration of a similar role for the plant cell wall is missing.

Cell fate regulation in *Arabidopsis* involves the atypical leucine-rich repeat receptor kinase STRUBBELIG (SUB). SUB, also known as SCRAMBLED (SCM), controls root hair specification (Fulton et al., 2009; Kwak et al., 2005) and regulates additional developmental processes, including floral morphogenesis and integument outgrowth (Chevalier et al., 2005; Lin et al., 2012). Present evidence indicates that SUB fulfills its role in these developmental processes in a complex with the transmembrane protein QUIRKY (QKY) (Fulton et al., 2009; Song et al., 2019; Trehin et al., 2013; Vaddepalli et al., 2014). Recent work has revealed that *SUB* also participates in the isoxaben-induced CWD response in young seedlings (Chaudhary et al., 2020). Interestingly, *QKY* was found to play only a minor role in this process. Moreover, *SUB*, *THE1*, and *MIK2* appear to function in different CBI-induced CWD pathways (Chaudhary et al., 2020).

Here, we report that *SUB* activity is regulated by the cell wall. We show that exposing plants to sub-lethal doses of isoxaben results in *sub*-like morphological defects. We also show that cell wall alterations eventually cause altered SUB complex architecture, increased endocytosis of SUB, and reduced *SUB* transcript levels.

[1]Plant Developmental Biology, TUM School of Life Sciences, Technical University of Munich, 85354 Freising, Germany. [2]Cell wall signaling group, Centre for Organismal Studies, University of Heidelberg, 69120 Heidelberg, Germany. *Present address: Department of Plant Biology, Carnegie Institution for Science, 260 Panama Street, Stanford, CA 94305, USA. ‡Present address: College of Life Sciences, Henan Normal University, Xinxiang, Henan 453007, People's Republic of China.

§Author for correspondence (kay.schneitz@tum.de)

A.C., 0000-0002-3719-4182; X.C., 0000-0002-5986-8838; R.B., 0000-0003-0825-6011; J.G., 0000-0002-6791-3838; S.W., 0000-0003-0832-6315; K.S., 0000-0001-6688-0539; K.S., 0000-0001-6688-0539

Handling Editor: Ykä Helariutta
Received 12 January 2021; Accepted 14 June 2021

Development (2021) 148, dev199425. doi:10.1242/dev.199425

Our data further reveal that ectopic upregulation of *SUB* expression counteracts the assayed morphological effects of cellulose deficiency.

RESULTS

Isoxaben reduces *SUB* expression levels

In light of the role of *SUB* in the CBI-induced CWD response (Chaudhary et al., 2020) we investigated whether isoxaben modulates *SUB* activity. To this end we made use of a well-characterized line carrying the *sub-1* null allele and a fully complementing transgene encoding a SUB:EGFP translational fusion driven by its endogenous promoter (pSUB::SUB:EGFP) (Gao et al., 2019; Vaddepalli et al., 2011, 2014). We observed considerably weaker pSUB::SUB:EGFP reporter signal in liquid-grown seedlings exposed to 600 nM isoxaben in comparison with reporter signal in mock-treated seedlings (Fig. 1A,B). Signal reduction could be detected from around 5 h after the start of the

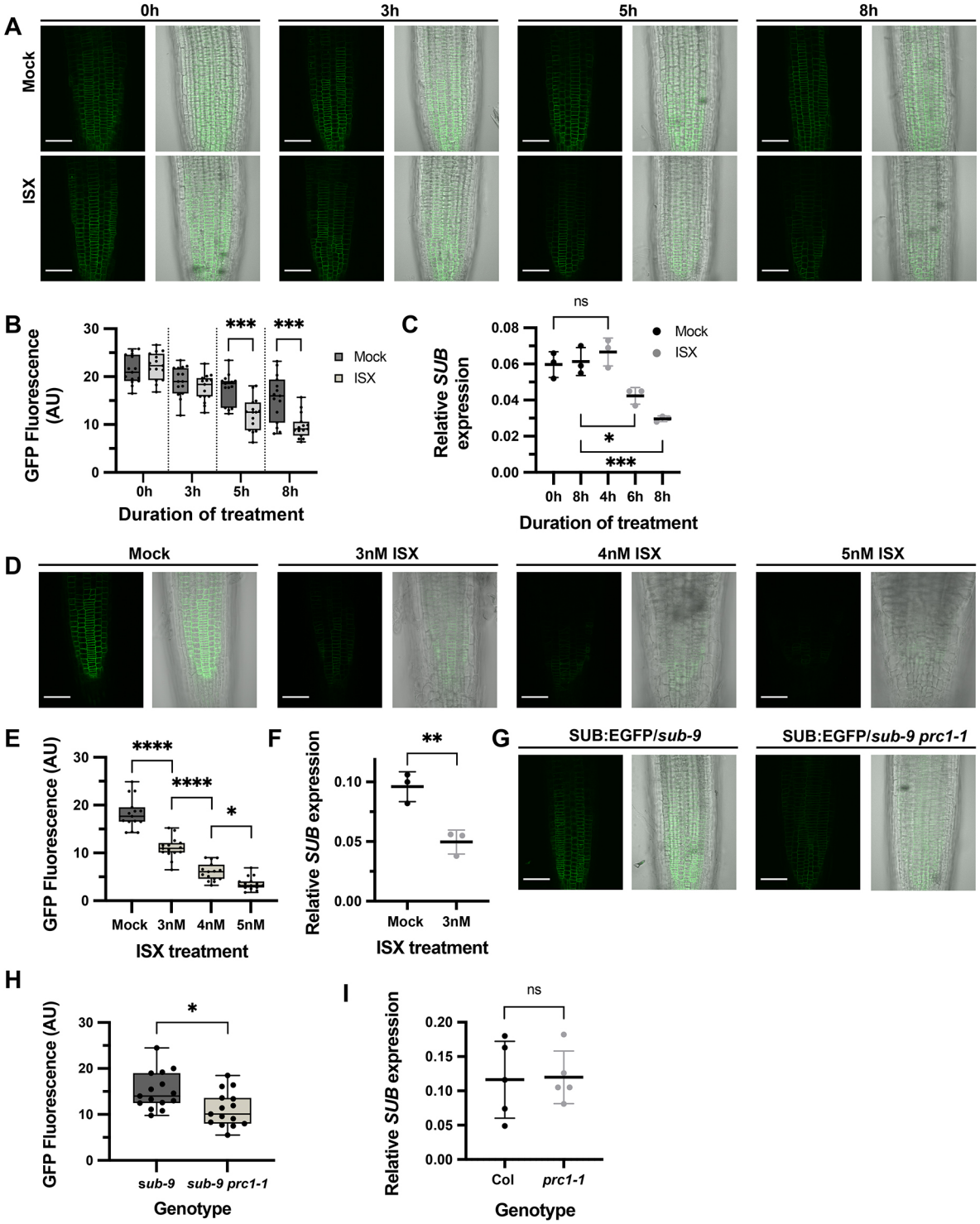

Fig. 1. See next page for legend.

Development (2021) 148, dev199425. doi:10.1242/dev.199425

Fig. 1. Effect of isoxaben treatment on *SUB* expression. (A) Signal intensity of a functional pSUB::SUB:EGFP reporter in *sub-1* upon exposure of liquid-grown seedlings to mock or 600 nM isoxaben. Note the reduction of signal in isoxaben-treated seedlings that starts at about 5 h of treatment. (B) Quantification of the data shown in A. n=15. ***P<0.0006; one-way ANOVA followed by post hoc Tukey's multiple comparison test. The experiment was performed three times with similar results. (C) Relative mRNA levels of *SUB* in 7-day-old seedlings exposed to mock or 600 nM isoxaben for 8 h. Expression was detected by qPCR. Data are mean±s.d., n=3 biological replicates each with mean of three technical replicates. *P<0.02; ***P=0.0007; one-way ANOVA followed by post hoc Tukey's multiple comparison test. The experiment was performed three times with similar results. (D) Signal intensity of a functional pSUB::SUB:EGFP reporter in *sub-1* upon exposure of plate-grown seedlings continuously exposed to mock or 3, 4 or 5 nM isoxaben. Note the reduced signal in isoxaben-treated seedlings. (E) Quantification of the data shown in D. n=15. ****P<0.0001; one-way ANOVA followed by post hoc Tukey's multiple comparison test. (F) Relative expression of *SUB* in 7-day-old seedlings grown on plates containing mock or 3 nM isoxaben. Expression was detected by qPCR. Data are mean±s.d., n=3 biological replicates each with mean of three technical replicates. **P<0.009; unpaired t-test with Welch's correction, two-tailed P-values. (G) Signal intensity of a functional pSUB::SUB:EGFP reporter in 7-day-old *sub-9* and *sub-9 prc1-1* plate-grown seedlings. Note the reduced signal in *sub-9 prc1-1* seedlings. (H) Quantification of the data shown in G. $n\leq$15. *P=0.0101; unpaired t-test with Welch's correction, two-tailed P-values. (I) Relative expression of *SUB* in 7-day-old seedlings grown on plates in Col and *prc1-1*. Expression was detected by qPCR. Data are mean±s.d., n=3 biological replicates each with mean of three technical replicates. ns, not significant; unpaired t-test with Welch's correction, two-tailed P-values. Box and whiskers plots show the median values (middle bars) and the 25th to 75th percentiles (box). The whiskers show the smallest and largest values. A, D and G show confocal micrographs depicting optical sections through the roots of 7-day-old seedlings. Imaging parameters between the mock and isoxaben treatments, or between genotypes, were identical. Experiments in B, E and H were performed three times with similar results. Scale bars: 50 µm.

treatment and was clearly evident after 8 h. Signal did not completely disappear but reached ∼50% of the intensity detected before the start of the isoxaben treatment. Importantly, reporter signal strength appeared unaltered in isoxaben-resistant *ixr2-1* seedlings carrying a mutation in the *CESA6* gene (Fig. S1) (Desprez et al., 2002; Heim et al., 1990a; Scheible et al., 2001). Furthermore, we detected significantly diminished endogenous *SUB* mRNA levels in seedlings treated with isoxaben for up to 8 h by quantitative real-time polymerase chain reaction (qPCR) in five out of six biological replicates (Fig. 1C). Transcript levels were noticeably reduced at the 6 h time point in three out of three biological replicates.

Next, we tested the effects of prolonged exposure of seedlings to isoxaben on SUB levels. *Arabidopsis* seedlings growing in the presence of isoxaben exhibited a response gamut ranging from near normal growth to essentially no growth in the narrow range of 1 to 10 nM isoxaben, with an I_{50} at 4.5 nM (Heim et al., 1989). Thus, we chose to analyze 7-day-old *sub-1 pSUB::SUB:EGFP* seedlings that were continuously grown on agar plates containing 3 nM, 4 nM and 5 nM isoxaben. In comparison with mock-treated samples we observed a concentration-dependent decrease in reporter signal in isoxaben-treated seedlings (Fig. 1D,E). A reduction in SUB:EGFP abundance was confirmed by western blot analysis (Fig. S2). We then assessed whether endogenous *SUB* transcript levels were affected in plate-grown wild-type seedlings exposed to 3 nM isoxaben for 7 days. We detected a reduction of *SUB* transcript levels by ∼50% in comparison to untreated seedlings (Fig. 1F).

PRC1 encodes the CESA6 subunit of cellulose synthase and the predicted null allele *prc1-1* shows reduced cellulose levels (Fagard et al., 2000). To assess whether SUB abundance is also diminished when cellulose biosynthesis is genetically perturbed, we generated a double mutant using the predicted null allele *sub-9* and *prc1-1*. The *sub-9 prc1-1* double mutant was made homozygous for the pSUB::SUB:EGFP reporter. We then compared the reporter signal in root tips of 7-day-old plate-grown seedlings of the strong *sub-9* mutant with that of the *sub-9 prc1-1* double mutant. We observed a noticeable reduction in reporter signal in *sub-9 prc1-1* in comparison with *sub-9* (Fig. 1G,H; Fig. S2). Next, we analyzed endogenous *SUB* transcript levels in wild-type and *prc1-1* seedlings by qPCR but we did not detect significant differences between the two genotypes (Fig. 1I).

We then investigated whether downregulation of *SUB* by isoxaben involves *QKY* function. We generated *pSUB::SUB:EGFP qky-8* plants and analyzed the signal of the pSUB::SUB:EGFP reporter in the roots of the respective plate-grown seedlings. We observed an additive effect on reporter signal strength when comparing untreated seedlings with seedlings exposed to isoxaben (Fig. S3). The result indicates that isoxaben and *QKY* affect SUB abundance through parallel pathways in seedling roots.

Cellulose biosynthesis inhibition affects SUB-complex architecture at the plasma membrane

The results mentioned above prompted us to investigate whether isoxaben influences the composition of SUB-containing protein complexes at the plasma membrane. Therefore, we assessed the steady-state fluorescence anisotropy of SUB:EGFP following mock or isoxaben treatment. Fluorescence anisotropy (r) describes the rotational freedom of a fluorescent molecule, such as GFP. Upon protein homo-oligomerization of GFP-based fusion proteins Förster resonance energy transfer (FRET) can occur (homo-FRET) resulting in a decrease in fluorescence anisotropy (Bader et al., 2011; Grossmann et al., 2018; Weidtkamp-Peters and Stahl, 2017). Monitoring changes in fluorescence anisotropy has been successfully applied in receptor kinase interaction studies involving for example CLV1 or BAK1 (Somssich et al., 2015; Stahl et al., 2013). As control, we used two lines carrying translational fusions of the TARGET OF MP5 (TMO7) transcription factor to one or three GFP moieties, respectively (Schlereth et al., 2010). We measured the fluorescence anisotropy values for the two fusion proteins in the nuclei of epidermal cells of the root meristem of plate-grown seedlings. We observed a fluorescence anisotropy of 0.38 for TMO7:1×GFP and 0.26 for TMO7:3×GFP (Fig. 2A,B,F). Free GFP in a plant cell has a steady-state anisotropy value of 0.33 (Somssich et al., 2015; Stahl et al., 2013). The higher anisotropy of TMO7:1×GFP indicates that this fusion protein is more restricted in its rotational freedom than free GFP. The low value for TMO7:3×GFP is indicative of homo-FRET between the three closely-linked GFP moieties.

We then determined the fluorescence anisotropy values for SUB:EGFP localized at the plasma membrane of epidermal cells of the root meristem. For comparison, we investigated two additional receptor kinases translationally fused to GFP and driven by their native promoters: THE1 and FERONIA (FER). THE1 and FER are both implied in monitoring the cell wall status (Cheung and Wu, 2011; Dünser et al., 2019; Feng et al., 2018; Hématy et al., 2007). In cells of untreated plate-grown seedlings we observed a fluorescence anisotropy value of 0.345 for SUB:EGFP, 0.355 for THE1:GFP and 0.352 for FER:GFP (Fig. 2C-F). The results could suggest that SUB:EGFP has a slightly higher rotational freedom in comparison to THE1:GFP and FER:GFP. Alternatively, differences in the linker sequences separating the kinase and GFP moieties of the three

Development (2021) 148, dev199425. doi:10.1242/dev.199425

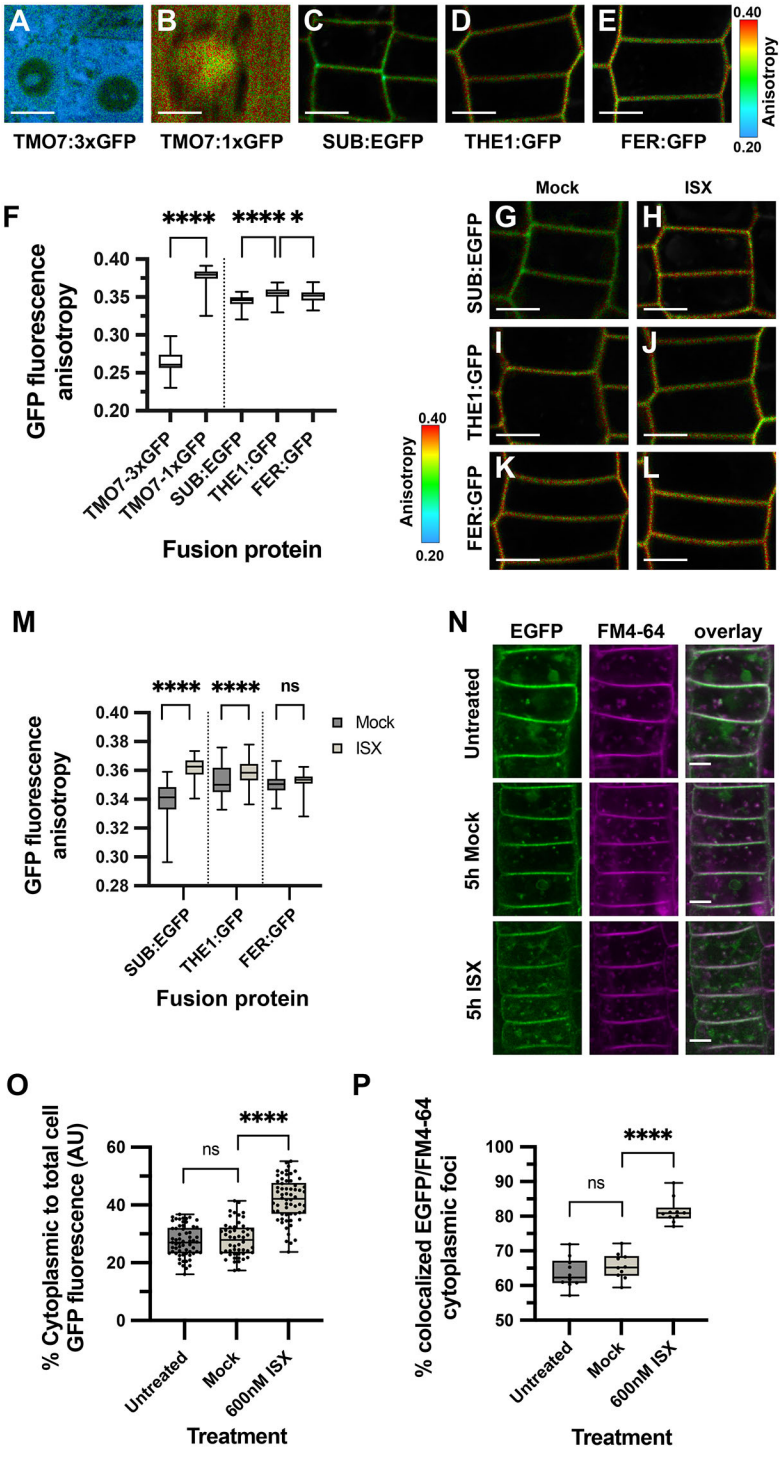

Fig. 2. Effect of isoxaben treatment on fluorescence anisotropy and sub-cellular localization of pSUB::SUB:EGFP. (A,B) Fluorescence anisotropy of TMO7:3×GFP and TMO7:1×GFP in cytoplasm. Note the increased anisotropy in TMO7:1×GFP (B). (C-E) Fluorescence anisotropy at the plasma membrane of the functional reporters pSUB::SUB:EGFP in *sub-1*, pTHE1::THE1:GFP (*the1-1*) and pFER::FER:GFP (*fer-4*). A minimum of 25 photons per anisotropy event were counted. (F) Quantification of the data shown in A-E. $150 \leq n \leq 169$. **P*<0.04; *****P*<0.0001; one-way ANOVA followed by Sidak's multiple comparison test. (G-L) Confocal micrographs depicting GFP-based fluorescence anisotropy in root epidermal cells of the meristematic region in 7-day-old seedlings after 4.5 h mock or 600 nM isoxaben treatment. Genotypes as in C-E. Imaging and fluorescence anisotropy calculation parameters were identical in C-E and G-L. A minimum of 25 photons per anisotropy event were counted. Note the increased anisotropy after isoxaben treatment in SUB:EGFP (G,H) and THE1::GFP (I,J). (M) Quantification of the data shown in G-L. $121 \leq n \leq 185$. *****P*<0.0001; one-way ANOVA followed by Sidak's multiple comparison test. (N) Fluorescence micrographs show optical sections of epidermal cells of root meristem of 7-day-old seedlings. Endocytic vesicles are marked by FM4-64. Note the increased SUB:EGFP signal in the cytoplasm as well as increased SUB:EGFP signal abundance in FM4-64 marked vesicles after isoxaben treatment. (O) Box and whisker plot depicting quantitative analysis of ratio of SUB:EGFP signal intensity in cytoplasm to total cells shown in N. $52 \leq n \leq 61$ cells from 10 different roots. *****P*<0.0001; one way ANOVA followed by Sidak's multiple comparison test. (P) Box and whisker plot depicting the result of colocalization analysis of SUB:EGFP and FM4-64 shown in N. *n*=10 roots, each data point represents a mean of at least five cells per root. *****P*<0.0001; one way ANOVA followed by Sidak's multiple comparison test. ns, not significant. Experiments in F, M, O and P were performed three times with similar results. Box and whiskers plots show the median values (middle bars) and the 25th to 75th percentiles (box). The whiskers show the smallest and largest values. A-E show confocal micrographs depicting fluorescence anisotropy of GFP in root epidermal cells of the meristematic region in 7-day-old seedlings. Scale bars: 5 µm.

fusion proteins could affect the fluorescence anisotropy values as they may influence the relative positions of the GFP moieties which in turn affects homo-FRET efficiency. We then analyzed the fluorescence anisotropy values of these reporters upon isoxaben treatment. Plate-grown seedlings were transferred onto Murashige and Skoog (MS) plates containing 600 nM isoxaben and incubated for 4.5 h. We observed a fluorescence anisotropy value for SUB:EGFP of 0.340 in mock-treated seedlings and a value of 0.361 upon isoxaben treatment (Fig. 2G-M). We scored fluorescence anisotropy values of 0.352 and 0.358 for THE1:GFP and 0.350 and 0.353 for FER:GFP, respectively. Thus, there is a noticeable difference in fluorescence anisotropy values for SUB:EGFP in mock versus isoxaben-treated cells. By contrast, we detected only minor alterations in these values for THE1:GFP and FER:GFP. The results indicate that SUB:EGFP-containing protein complexes experience different architectures depending on the presence or absence of isoxaben-induced CWD.

Perturbation of cellulose biosynthesis promotes internalization of SUB

We then tested whether isoxaben treatment affects the subcellular distribution of the pSUB::SUB:EGFP reporter signal in epidermal

Development (2021) 148, dev199425. doi:10.1242/dev.199425

cells of the root meristem (Fig. 2N-P). In untreated seedlings SUB is known to undergo ubiquitylation and continuous internalization (Gao et al., 2019; Song et al., 2019). We found that the percentage of cytoplasmic SUB:EGFP foci increased upon isoxaben treatment in comparison with untreated or mock-treated cells (Fig. 2N,O). To assess whether the accumulation of cytoplasmic SUB:EGFP foci upon isoxaben treatment related to endocytosis we imaged cells of seedlings that were exposed to the different types of treatment upon a 5-min incubation with the endocytic tracer dye FM4-64. Applying a convenient criterion for colocalization (Gao et al., 2019; Ito et al., 2012), the internal SUB:EGFP and FM4-64 signals were considered colocalized when the distance between the centers of the two types of signals was below the limit of resolution of the objective (0.24 µm). In untreated or mock-treated seedlings we observed that 63.7% (n=322) and 65.6% (n=536), respectively, of all cytoplasmic SUB:EGFP foci were also marked by FM4-64, confirming the previous observation that SUB:EGFP undergoes recognizable internalization in the absence of any apparent stimulation (Gao et al., 2019). Upon isoxaben treatment, we noticed that 81.5% (n=633) of all cytoplasmic SUB:EGFP foci were also marked by FM4-64. These data support the notion that isoxaben treatment eventually leads to increased endocytosis of SUB:EGFP.

Exposing plants to sub-lethal doses of isoxaben induces root hair patterning defects

As isoxaben treatment results in the downregulation of *SUB* we investigated whether isoxaben treatment of wild-type plants results in a *sub*-like phenotype. In a first step we explored whether application of isoxaben induces root hair patterning defects in 7-day-old seedlings. We compared the number of hair (H) and nonhair (N) cells in the N and H positions of the root epidermis, respectively, in untreated and treated wild-type seedlings to the respective numbers in untreated *sub-9* roots (Fig. 3; Table 1). In untreated plate-grown wild-type plants, we found that 97.1% of cells at the H position were hair cells whereas only 3.7% of cells at the N position were hair cells (Fig. 3A). In contrast, in mock-treated *sub-9* seedlings only 71.1% of cells at the H position were hair cells and 23.4% of cells at the N position were hair cells (Fig. 3B), confirming previous results (Kwak et al., 2005). Wild-type seedlings grown on 3 nM isoxaben plates for 7 days exhibited 68.0% hair cells in the H position and 25.1% hair cells in the N position (Fig. 3C,D). We also found that treating *sub-9* seedlings with 3 nM isoxaben plates resulted in similarly strong defects (Table 1), suggesting that application of isoxaben did not noticeably enhance the root hair patterning defect in *sub-9*. Root hair patterning appeared unaltered in mock or isoxaben-treated *ixr2-1* mutants (Fig. 3E,F). To test whether a genetic defect in cellulose biosynthesis results in aberrant root hair patterning we analyzed *prc1-1* mutants. We observed a mild but robust difference in root hair patterning in comparison with the wild type (Fig. 3G).

Next, we tested whether the altered root hair patterning is reflected at the molecular level (Fig. 3H-N; Table 2). We made use of Col-0 plants carrying a pGL2::GUS:GFP reporter. The *GLABRA2* (*GL2*) promoter drives expression in N cells but not in H cells of the root epidermis (Duckett et al., 1994), and the expression pattern of a reporter driven by the *GL2* promoter thus serves as a convenient and faithful proxy for root hair patterning (Gao et al., 2019; Kwak et al., 2005; Masucci et al., 1996). Seedlings were first grown on MS plates for 5 days and then transferred to mock plates or plates containing 1-3 nM isoxaben for 48 h. As expected, mock-treated wild-type seedlings showed the

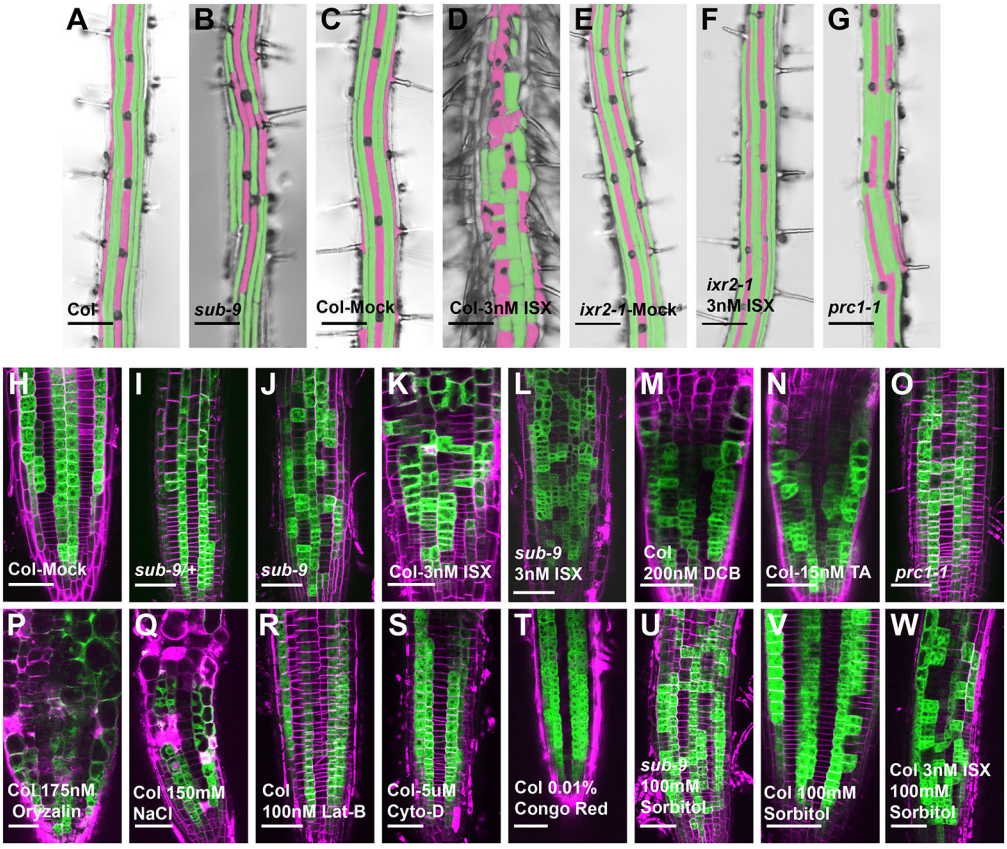

Fig. 3. Reduced cellulose biosynthesis results in altered root hair cell patterning. (A-G) Micrographs show epidermal root hair cell patterning in 7-day-old seedlings in the presence or absence of isoxaben. Pink and green colors mark root hair cells and non-root hair cells, respectively. Note the straight-line arrangement of hair cells. For a quantification, see Table 1. The experiment was performed three times with similar results. (H-W) Confocal micrographs depicting the epidermal cell layer of roots of 7-day-old seedlings showing pGL2::GUS:GFP reporter signal. The cell wall was counter-stained with propidium iodide, except for T. For a quantification of the aberrant effects see Table 2. The experiment was performed three times with similar results. Genotypes and/or treatments are indicated in the panels. Scale bars: 100 µm (A-G); 50 µm (H-W).

Development (2021) 148, dev199425. doi:10.1242/dev.199425

Table 1. Distribution of root hair and nonhair cells in the root epidermis

		H position‡			N position‡		
Genotype/Treatment	Roots*	Cells total	Hair (%)	Nonhair (%)	Cells total	Hair (%)	Nonhair (%)
Col-0/Mock	17	321	97.1±3.4	2.9±3.4	472	2.0±2.9	98.0±2.9
Col-0/3 nM ISX	17	442	68.0±5.0	32.0±5.0	601	25.1±6.1	74.9±6.1
sub-9/Mock	17	435	71.1±4.2	28.9±4.2	612	23.4±4.2	76.6±4.2
sub-9/3 nM ISX	20	535	69.7±8.8	30.3±8.8	539	29.1±7.7	70.9±7.7
ixr2-1/Mock	15	204	94.5±6.9	5.5±6.9	341	3.9±3.8	96.1±3.8
ixr2-1/3 nM ISX	15	262	94.9±5.2	5.1±5.2	346	5.7±5.0	94.3±5.0
Col-0	15	414	97.1±3.4	2.9±3.4	550	3.7±2.6	96.3±2.6
prc1-1	15	291	83.4±3.0	16.6±3.0	373	13.4±4.2	86.6±4.2

*Total number of different roots analyzed.

‡Data are mean±s.d. Two-tailed Mann–Whitney tests revealed significant differences (P<0.0001) for the following comparisons: Col/mock versus Col/3 nM isoxaben (ISX), Col/mock versus *sub-9*/mock, Col/mock versus *sub-9*/3 nM ISX, Col versus *prc1-1*, *sub-9*/mock versus *prc1-1*. Two-tailed Mann–Whitney tests failed to reveal significant differences (P>0.2) for the following comparisons: Col versus Col/mock, *sub-9*/mock versus *sub-9*/3 nM ISX, *sub-9*/3 nM ISX versus Col/3 nM ISX, Col/mock versus *ixr2-1*/mock, Col/mock versus *ixr2-1*/3 nM ISX, *ixr2-1*/mock versus *ixr2-1*/3 nM ISX.

The experiment was repeated twice with similar results.

regular spatial expression pattern (Fig. 3H). Mock-treated *sub-9*/+ heterozygotic seedlings showed mild defects in reporter expression, revealing a weak haploinsufficiency of *SUB* and indicating that SUB levels are important to its function (Fig. 3I). Mock-treated *sub-9* homozygous seedlings clearly exhibited an altered expression pattern (Fig. 3J; Table 2). Upon exposing wild-type seedlings to 1-3 nM isoxaben we found a pronounced and concentration-dependent increase in defects in the expression pattern of the reporter (Fig. 3K; Table 2). The prominent misexpression resembled the expression pattern of the reporter in *sub-9* mutants (Fig. 3J,K; Table 2). Isoxaben-treated *sub-9* seedlings showed an effect that was comparable with the one shown by mock-treated *sub-9* seedlings (Fig. 3L; Table 2). We similarly treated wild-type seedlings with 200 nM 2,6-dichlorobenzonitrile (DCB) or 15 nM Thaxtomin A, two other cellulose biosynthesis inhibitors (Heim et al., 1990b; Scheible et al., 2003; Tateno et al., 2016). Both drugs induced *sub*-like expression pattern defects of the pGL2::GUS:GFP reporter (Fig. 3M,N; Table 2). Moreover, we observed that *prc1-1* mutants exhibited a mild but noticeable aberration in the expression pattern of the reporter (Fig. 3O). Thus, plants treated with three different cellulose inhibitors and a cellulose biosynthesis mutant all exhibit aberrant spatial expression of the pGL2::GUS:GFP reporter.

Cortical microtubules direct the movement of CSCs (Paredez et al., 2006). Salt stress leads to microtubule disassembly followed by the formation of a stress-tolerant microtubule network required for sustained cellulose synthesis during salt stress (Endler et al., 2015; Wang et al., 2011). In addition, regular cell wall deposition depends on the actin cytoskeleton (Crowell et al., 2009; Gutierrez et al., 2009; Sampathkumar et al., 2013). Thus, we explored whether drugs affecting the cytoskeleton had an effect on the pGL2::GUS:GFP expression pattern. We tested seedlings grown for 5 days on MS plates followed by exposure for 48 h to 175 nM oryzalin, 150 mM NaCl, 100 nM latrunculin B or 5 µM Cytochalasin D, respectively. In all instances we did not notice an obvious effect on the pGL2::GUS:GFP expression pattern (Fig. 3P-S) although the applied drug concentrations affect the organization of microtubules and actin filaments (Baskin et al., 1994; Ketelaar et al., 2003; Staiger et al., 2009). We also tested whether application of Congo Red, a stain that allows the detection of cellulose microfibrils (Verbelen and Kerstens, 2000) and that possibly interferes with their organization, has an effect on the pGL2::GUS:GFP pattern. We did not observe a noticeable effect upon staining with Congo Red (Fig. 3T).

The isoxaben-induced CWD response is generally sensitive to turgor pressure (Hamann et al., 2009). We investigated whether the effect of isoxaben on root hair patterning follows the same pattern (Fig. 3U-W; Table 2). We thus analyzed pGL2::GUS:GFP reporter expression in sorbitol-treated *sub-9* or wild-type seedlings and wild-type seedlings simultaneously exposed to isoxaben and sorbitol. We found that application of sorbitol did not influence the reporter patterns in *sub-9* or wild-type seedlings (Fig. 3U,V). In addition, we found that reporter expression remained aberrant in wild-type seedlings exposed to isoxaben and sorbitol (Fig. 3W), suggesting that the isoxaben-induced effect on root hair patterning is not sensitive to alterations in turgor pressure. Thus, these data indicate that the CWD-sensitive mechanism controlling *SUB* expression levels is distinct from the regulation of other CBI-induced CWD responses, including callose accumulation, cell cycle gene expression or root cell shape changes (Engelsdorf et al., 2018; Gigli-Bisceglia et al., 2018; Hamann et al., 2009).

Exposing plants to sub-lethal doses of isoxaben induces *sub*-like floral defects

To explore further the effect of isoxaben on tissue morphogenesis we tested whether isoxaben treatment also induces *sub*-like defects in flowers and ovules. We compared wild-type (L*er*) and *sub-1* plants that were cultivated on soil in the presence of isoxaben. Plants were initially grown without any treatment. Just before bolting we began watering wild-type plants with 100-500 nM isoxaben and continued watering with isoxaben in 3-day intervals for 2 weeks. We then analyzed stage 3 floral meristems (stages according to Smyth et al., 1990; Fig. 4A-C). Floral meristems of *sub-1* mutants show aberrant cell division planes in the L2 layer (Chevalier et al., 2005; Fulton et al., 2009). Analysis of floral meristems of isoxaben-treated wild-type Col-0 plants revealed similar defects (Fig. 4B) the frequency of which increased with increasing concentrations of isoxaben (Table 3). Next, we compared stage 13 flowers of isoxaben-treated L*er* plants with flowers from untreated *sub-1* plants (Fig. 4D-F). We noticed that flowers from isoxaben-treated plants exhibited a *sub*-like altered arrangement of petals. Finally, we analyzed the ovule phenotype of isoxaben-treated wild-type plants. We observed *sub*-like defects in integument outgrowth in late stage 3 or early stage 4 ovules (ovule stages according to Schneitz et al., 1995; Fig. 4G-I; Table 4). The frequency and severity of the integument defects also depended on the concentration of isoxaben (Table 4).

Development (2021) 148, dev199425. doi:10.1242/dev.199425

Table 2. Position-dependent pattern of pGL2::GUS:GFP reporter expression in root epidermal cells upon a 48 h exposure to isoxaben

Genotype	Treatment	H cells total*	H position‡,§,¶	N cells total*	N position‡
Col	–	633	3.0±2.8	741	96.4±3.6
sub-9/+	–	580	10.6±3.2	688	90.6±2.4
sub-9	–	548	33.6±9.2	615	75.3±5.4
Col	1 nM ISX	441	14.1±4.2	589	86.1±6.1
	2 nM ISX	375	26.7±9.4	459	78.3±3.2
	3 nM ISX	395	30.5±6.6	579	77.4±7.1
sub-9	3 nM ISX	519	37.8±4.6	504	74.8±4.5
Col	200 nM DCB	334	29.5±7.2	488	70.7±7.4
Col	15 nM TA	352	27.9±6.2	484	71.4±6.0
prc1-1	–	543	9.5±2.2	699	91.0±2.4
sub-9	100 mM sorbitol	506	31.5±8.7	619	74.0±7.6
Col	100 mM sorbitol	475	3.0±3.0	571	97.1±2.1
Col	3 nM ISX 100 mM sorbitol	453	30.0±6.4	573	75.9±7.0
SUB OE L1	–	423	7.2±4.8	558	77.4±4.4
	1 nM ISX	616	4.2±3.5	663	95.8±2.2
	2 nM ISX	327	1.2±2.2	396	92.5±3.4
	3 nM ISX	401	16.9±6.3	445	87.2±5.2
SUB OE O3	–	508	4.5±4.5	701	82.3±4.6
	1 nM ISX	638	3.7±3.4	706	94.7±2.6
	2 nM ISX	320	3.2±3.9	396	92.9±5.8
	3 nM ISX	359	11.3±5.1	475	86.9±5.1

For each genotype and treatment 10 different roots of 7-day-old seedlings were analyzed. The experiment was performed twice with similar results.
*Total number of cells at H or N position scored.
‡Percentage of cells at H or N position expressing the pGL2::GUS:GFP reporter.
§Two-tailed Mann–Whitney tests revealed significant differences for the following comparisons: Col versus *sub-9*/+, Col versus *prc1-1* ($P<0.002$); Col versus *sub-9*, Col versus Col/200 nM DCB, Col versus 10 nM TA, Col versus Col/1-3 nM isoxaben (ISX) ($P<0.0001$); Col/1-3 nM ISX versus SUB OE L1/1-3 nM ISX (equivalent treatments were compared, $P<0.0002$); Col/1-3 nM ISX versus SUB OE O3/1-3 nM ISX (equivalent treatments were compared, $P<0.0001$).
¶Two-tailed Mann–Whitney tests failed to reveal significant differences for the following comparisons: *sub-9*/+ versus *prc1-1*, *sub-9* versus *sub-9*/3 nM ISX, *sub-9* versus Col/3 nM ISX, *sub-9* versus *sub-9*/100 mM sorbitol, Col/3 nM ISX versus Col/3 nM ISX+100 mM sorbitol ($P>0.4$).

Ectopic expression of *SUB* attenuates the detrimental effects of isoxaben on root hair patterning and floral development

If isoxaben treatment results in a downregulation of *SUB* and a *sub*-like phenocopy, ectopic expression of *SUB* should counteract this outcome. We tested this hypothesis by analyzing the effects of isoxaben on two well-characterized lines carrying a pUBQ::SUB:mCherry transgene (lines L1 and O3) (Chaudhary et al., 2020) (Fig. S4). To this end we generated L1 and O3 lines homozygous for the pGL2::GUS:GFP construct. We then analyzed reporter signal in 7-day-old plate-grown seedlings that had been grown on regular MS plates for 5 days before being transferred to mock plates or plates containing 1 nM, 2 nM or 3 nM isoxaben for another 48 h before analysis (Fig. 5A-D; Table 2).

Ectopic expression of *SUB* in *p35S::SUB* plants results in aberrant pGL2::GUS expression and a mild defect in root hair patterning (Kwak and Schiefelbein, 2007). It is unclear why loss-of-function or overexpression of *SUB* results in root hair patterning defects but may relate to the proposed role of SUB acting as a scaffold in a multi-protein complex, the stoichiometry of which may be important (Chaudhary et al., 2020). Confirming this finding, we found that L1 and O3 showed an altered expression pattern of the pGL2::GUS:GFP reporter in roots of untreated seedlings, with more cells in the H position and fewer cells in the N position exhibiting reporter signal compared with wild type (Fig. 5A; Table 2). In the case of the isoxaben-treated L1 and O3 lines we detected significant differences to wild type. Exposing seedlings of L1 and O3 to 1 or 2 nM isoxaben resulted in pGL2::GUS:GFP patterns that resembled the pattern observed in untreated wild-type seedlings and that were less aberrant than the pGL2::GUS:GFP patterns observed in corresponding isoxaben-treated wild-type seedlings (Fig. 5B-D; Table 2). Moreover, the defects were weaker when compared with the aberrations exhibited by untreated L1 and O3. Exposing L1 or O3 seedlings to 3 nM isoxaben resulted in defects that were still less severe in comparison with wild-type plants treated with 3 nM isoxaben (Table 2).

Finally, we tested whether ectopic expression of *SUB* also alleviated the effects of isoxaben on floral development by cultivating lines L1 and O3 in the presence of different concentrations of isoxaben as described above. We found that the defects in floral meristem organization, petal arrangement and ovule development were noticeably reduced in both lines compared with wild type (Fig. 5E-H; Tables 3, 4).

DISCUSSION

The extracellular matrix in animal cells not only provides structural support but also exerts additional functions, including developmental patterning, as in the control of epidermal stem cell fate (Hynes, 2009; Watt and Fujiwara, 2011). By contrast, the role of the plant cell wall in the regulation of cell fate is less well explored. The presented results strongly indicate that alterations in cell wall composition induced by the herbicide isoxaben or genetically in *prc1-1* mutants are associated with defects in root hair patterning in the root epidermis. Thus, they demonstrate a role of the plant cell wall in the control of root hair cell fate.

The combined data indicate a shared molecular framework underlying cell-wall-mediated regulation of root hair cell fate, floral morphogenesis and ovule development that involves the control of the atypical receptor kinase SUB, a well-known regulator of these developmental processes (Chevalier et al., 2005; Fulton et al., 2009; Kwak and Schiefelbein, 2007; Kwak et al., 2005). We found that exposure of seedlings to sub-lethal concentrations of isoxaben affects the architecture of SUB:EGFP-containing protein complexes at the plasma membrane, leads to increased internalization of SUB:

Development (2021) 148, dev199425. doi:10.1242/dev.199425

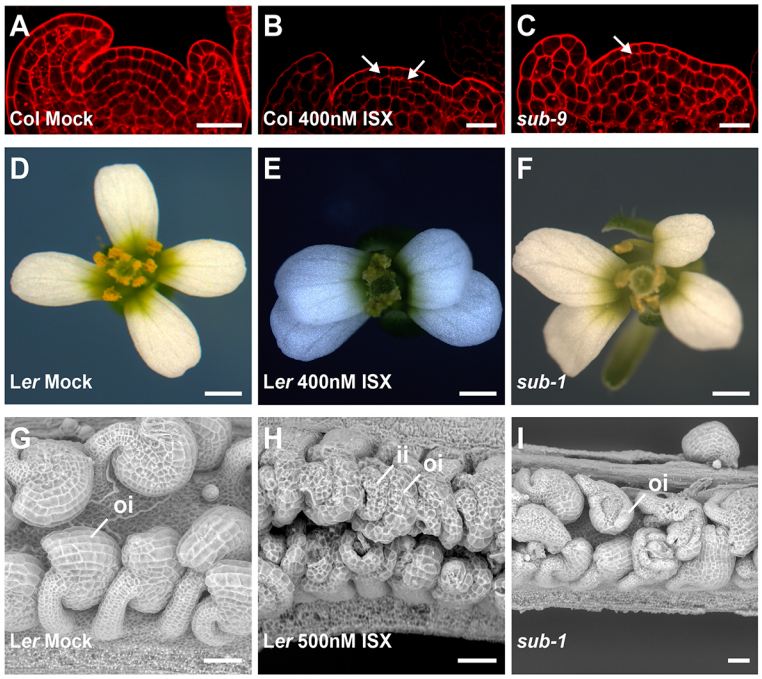

Fig. 4. Effect of isoxaben treatment on floral and ovule morphogenesis. (A-C) Confocal micrographs depicting mid-optical sections through stage 3 floral meristems stained with propidium iodide. Arrows indicate irregular periclinal cell divisions in L2. For a quantification of the effects see Table 3. (D-F) Morphology of mature stage 13 or 14 flowers. Compare E and F with D and note the aberrant arrangement of petals. Of those flowers examined, 87% (13/15) showed the phenotype in D, 82% (18/22) showed the phenotype in E and 71% (12/17) showed the phenotype in F. The experiment was repeated twice with similar results. (G-I) Electron scanning micrographs depicting mature stage 3 or 4 ovules. For a quantification of the effects see Table 4. Compare to H and I with G and note aberrant integuments. Genotypes and/or treatments are indicated in the panels and Table 4. Scale bars: 20 µm (A-C); 0.5 mm (D-F); 50 µm (G-I).

EGFP and causes a dose-dependent reduction in *SUB* transcript levels. Importantly, application of isoxaben did not enhance the root hair patterning defect in *sub-9* null mutants, indicating that isoxaben affects root hair cell fate mainly through downregulation of SUB. Moreover, ectopic expression of SUB:mCherry attenuated the detrimental effects of isoxaben on all the investigated developmental processes, providing further support for the notion that the isoxaben-induced decrease in SUB abundance is of biological relevance. Thus, the collective evidence suggests that the control of SUB levels by the cell wall is a central aspect of *SUB*-mediated signal transduction.

Our data expose a quantitative effect of cellulose reduction on SUB expression levels and concomitantly reveal that different levels of SUB are limiting for different *SUB*-dependent processes. We propose that the regulation of root hair patterning or floral morphogenesis depends on higher levels of SUB, whereas the CBI-induced compensatory CWD response in seedlings requires only a basal level of SUB. This is supported by the observation that exposure of seedlings to sub-lethal doses of isoxaben resulted in reduced *SUB* transcript levels in seedlings and prominent defects in root hair patterning. Under such conditions the *SUB*-dependent CBI-induced CWD response remains operational (Chaudhary et al., 2020). Moreover, *QKY* is essential for *SUB*-mediated root hair patterning, floral morphogenesis and ovule development (Fulton et al., 2009; Song et al., 2019; Trehin et al., 2013; Vaddepalli et al., 2014). However, with the exception of lignin accumulation, *QKY* is not required for the *SUB*-mediated CBI-induced CWD response (Chaudhary et al., 2020), despite the fact that SUB abundance is noticeably reduced in *qky* seedlings (Song et al., 2019) (Fig. S3). Interestingly, we observed a reduction in pSUB::SUB:EGFP signal in *prc1-1* while *SUB* transcript levels were unaltered. The finding suggests that a decrease in functional SUB protein levels is sufficient to lead to mild defects in root hair patterning. Further evidence for a limiting role for SUB in this process is provided by the observation that *sub-9* heterozygotes exhibit a *prc1-1*-like root hair patterning phenotype (Fig. 3I,O; Table 2). Thus, we propose that the different functions of SUB relate to different levels of SUB and the presence of SUB complexes with diverse architectures at the plasma membrane.

Table 3. Number of periclinal cell divisions in L2 layer of stage 3 floral meristems of plants exposed to different concentrations of isoxaben

Genotype	ISX [nM]*	FM‡	PCD§	Percentage¶
Col	0	29	5	17.2
sub-9	0	31	14	45.2
Col	200	14	4	28.6
	300	21	8	38.1
	400	25	15	60.0
SUB OE L1	0	8	2	25.0
	400	27	6	22.2

*Isoxaben (ISX) concentration in water.
‡Number of floral meristems analyzed.
§Number of periclinal cell divisions observed.
¶Two-sided Chi-squared tests revealed significant differences (P<0.02) for the following comparisons: Col versus *sub-9*, Col versus Col/400 nM ISX, Col/400 nM ISX versus SUB OE L1/400 nM ISX.
The experiment was performed twice with similar results.

The differential effects of *PRC1* and isoxaben on *SUB* transcript levels are consistent with the notion that the control of *SUB* includes at least two distinct processes that react to variations in the CWD signal: post-transcriptional regulation and control of *SUB* transcript levels. A comparably low reduction in cellulose content would originate a CWD signal that leads to increased SUB internalization. A more pronounced drop in cellulose content would elicit a stronger or different CWD signal that would further affect *SUB* transcript levels. The stronger effect of higher concentrations of isoxaben in comparison with *prc1-1*, which carries a mutation in the *CESA6* gene (Fagard et al., 2000), is explained by the observation that isoxaben affects several primary cell wall CESA subunits (Desprez et al., 2002; Heim et al., 1990a; Scheible et al., 2001). Moreover, *CESA6* function is buffered by redundantly acting *CESA6*-like genes (Desprez et al., 2007; Persson et al., 2007).

There is crosstalk between cell wall components (Cosgrove, 2018). For example, plants with a defect in hemicellulose production or in pectin methylation exhibit reduced cellulose

Development (2021) 148, dev199425. doi:10.1242/dev.199425

Table 4. Comparison of integument defects of Col, *sub-9*, *sub-21* and Col plants exposed to different concentrations of isoxaben

Genotype	ISX [nM]*	Ovules‡	Defective ovules§,¶
Col	0	502	0.0
sub-9	0	629	44.2
sub-21	0	578	49.5
Col	200	547	13.5
	300	576	25.4
	400	563	34.3
	500	551	50.5
SUB OE L1	0	511	0.0
	200	593	2.4
	300	527	4.0
	400	573	8.7
	500	581	14.1
SUB OE O3	0	570	0.0
	200	587	1.9
	300	508	3.3
	400	571	8.4
	500	541	16.1

For each genotype and treatment at least 15 different carpels from four different plants were analyzed.
*Isoxaben (ISX) concentration in water.
‡Total number of ovules scored.
§Percentage of ovules with *sub*-like integument defects.
¶Statistical significance $P<0.0001$: Col versus *sub-9* or *sub-21*; Col versus Col/200-500 nM ISX; Col/200-500 nM ISX versus SUB OE L1/200-500 nM ISX or SUB OE O3/200-500 nM ISX. Equivalent treatments were compared. Significance was estimated by a two-sided Fisher's exact test. Similar values were obtained with a two-sided Chi-squared test. The experiment was performed three times with similar results.

content (Du et al., 2020; Xiao et al., 2016). Indeed, we found that *SUB* transcript and SUB:EGFP protein levels were downregulated upon application of epigallocatechin gallate (EGCG), an inhibitor of pectin methylesterase activity (Lewis et al., 2008), to 7-day-old seedlings. Moreover, the treated seedlings exhibited root hair patterning defects (Fig. S5). The relative influence of altered pectin architecture and reduced cellulose content on these processes remains to be investigated.

The signal that controls SUB internalization and *SUB* transcript levels is currently unknown, but the cell wall represents an obvious possible source. However, movements of CSCs are guided by cortical microtubules (Paredez et al., 2006) and several components of CSCs interact with microtubules (Bringmann et al., 2012; Endler et al., 2015; Gu et al., 2010; Kesten et al., 2019; Liu et al., 2016; Li et al., 2012). Application of isoxaben results in the rapid internalization of CESA subunits (Paredez et al., 2006) and isoxaben-treated wild-type plants as well as several cesa mutants were shown to exhibit altered cortical microtubule alignment (Chu et al., 2007; Fisher and Cyr, 1998; Paredez et al., 2008). Thus, the signal regulating SUB abundance could also originate from the cytoskeleton. However, we think it unlikely as treatment of seedlings with pharmaceutical compounds affecting the microtubule or actin cytoskeleton did not result in noticeable aberrations in root hair patterning. It will be interesting to identify the cell wall-derived signal in future studies.

MATERIALS AND METHODS

Plant work and lines

Arabidopsis (L.) Heynh. var. Columbia (Col-0) and var. Landsberg (*erecta* mutant) (L*er*) were used as wild-type strains. Plants were grown on soil as previously described (Fulton et al., 2009). Plate-grown seedlings were grown in long-day conditions (16 h light/8 h dark) on half-strength Murashige and Skook (1/2 MS) agar plates supplemented with 0.3% sucrose. The following mutant alleles were used: *sub-1* and *qky-8* (L*er*) and *sub-9* and *sub-21* (Col) (Chaudhary et al., 2020; Chevalier et al., 2005; Fulton et al., 2009), *prc1-1* (Col) (Fagard et al., 2000), *ixr2-1* (Col) (Desprez et al., 2002). The *sub-1*, *sub-9* and *sub-21* alleles all represent predicted null alleles that cause comparable defects in root hair patterning and ovule development. The lines carrying pSUB::SUB:GFP, pUBQ::SUB:mCherry (O3, L1, Col) and pGL2::GUS:GFP (Col) have been previously reported (Chaudhary et al., 2020; Gao et al., 2019; Vaddepalli et al., 2011, 2014). The pTHE1::THE1:GFP line was a gift from Herman Höfte (INRA, AgroParisTech, Versailles, France). The pFER::FER:GFP (Duan et al., 2010) as well as the TMO7:1×GFP and TMO7:3×GFP reporter lines (Schlereth et al., 2010) have been previously described. For the generation of the various multiple mutant lines see supplementary Materials and Methods for further details.

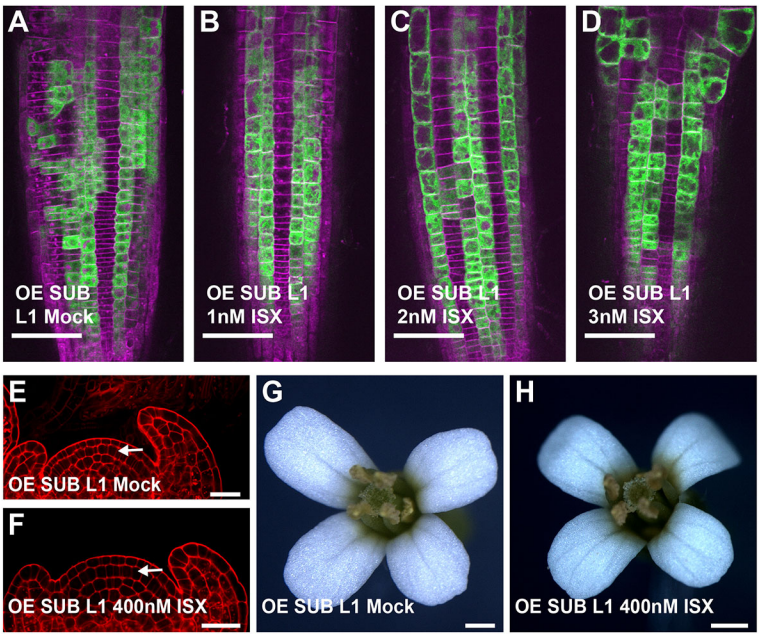

Fig. 5. Overexpression of SUB:mCherry attenuates the isoxaben effects on root hair patterning and floral morphogenesis. (A-D) Confocal micrographs depicting optical sections through roots of 7-day-old seedlings showing the pGL2::GUS:GFP expression pattern. The cell wall was counter-stained with propidium iodide. Note the mild aberration in pGL2::GUS:GFP pattern in A (compare with Fig. 3H). Note the normal to mildly abnormal pGL2::GUS:GFP patterns in B-D (compare with Fig. 3I). For a quantification of the effects see Table 2. The remaining roots showed the occasional single cell displacement in the reporter expression as also sometimes seen in wild type (Table 2). The experiment was performed three times with similar results. (E,F) Confocal micrographs depicting mid-optical sections through stage 3 floral meristems stained with propidium iodide. For a quantification of the effects see Table 3. Arrows highlight regular L2 layers. (G,H) Morphology of stage 13 or 14 flowers. Note the normal petal arrangement. Of those flowers examined, 74% (14/19) showed the phenotype in G and 82% (18/22) showed the phenotype in H. The experiment was repeated twice with similar results. Genotypes and/or treatments are indicated in the panels. Scale bars: 50 µm (A-D); 20 µm (E,F); 0.5 mm (G,H).

Development (2021) 148, dev199425. doi:10.1242/dev.199425

Chemical treatments

Isoxaben, DCB, Thaxtomin A, Latrunculin B, Cytochalasin D, oryzalin, sorbitol, Congo Red and EGCG were obtained from Sigma-Aldrich and used from stock solutions in DMSO (isoxaben: 100 µM; DCB: 1 mM; Thaxtomin A: 100 µM; Latrunculin B: 100 µM; Cytochalasin D: 500 µM; Oryzalin: 100 µM; EGCG: 1 mM) or in water (sorbitol: 1 M; NaCl: 2.5 M; Congo Red: 1%). FM4-64 was purchased from Molecular Probes (2 mM stock solution in water). For FM4-64 staining seedlings were incubated in 4 µM FM4-64 in liquid 1/2 MS medium for 5 min before imaging.

PCR-based gene expression analysis

For qPCR of *SUB*, 35-40 seedlings per flask were grown in liquid culture under continuous light at 18°C for 7 days, followed by treatment with mock or 600 nM isoxaben for 8 h on plates (21°C, long-day conditions). RNA extraction and quality control were performed as previously described (Box et al., 2011). cDNA synthesis, qPCR and analysis were carried out essentially as previously described (Enugutti et al., 2012). Primers are listed in Table S1.

Western blot analysis

We collected 300 mg of 7-day wild-type or mutant *Arabidopsis* seedlings with forceps, placed them in a 2 ml Eppendorf tube and froze them immediately using liquid nitrogen. After lyzing the seedlings using a Tissue Lyser (Qiagen), two volumes of 2× Laemmli buffer [65.8 mM Tris-HCl (pH 6.8), 2.1% (w/v) SDS, 26.3% (v/v) glycerol, 2.5% (v/v) β-mercaptoethanol, 0.01% bromophenol blue] were added to the homogenate. Samples were boiled at 70°C for 15 min, centrifuged at 12,000 rpm (10,625 ***g***) for 20 min, and the supernatant was loaded on the gel. Proteins separated in SDS-10% PAGE were transferred to a PVDF membrane using the Trans-Blot Turbo Transfer System (Bio-Rad). Membranes were blocked with blocking buffer [2.5% milk powder in TBS-T (50 mM Tris-Cl, 150 mM NaCl, 0.1% Tween-20, pH 7.4)] and incubated with a GFP-antibody (3H9, Chromotek, 1:2500) at 4°C. Anti-rat horseradish peroxidase-conjugated antibody was used as a secondary antibody (AS10 1187, Agrisera, 1:5000). Blots were developed using chemiluminescence (Supersignal West Atto, Thermo Fisher Scientific) and stained afterwards with Ponceau S for assessing loading.

Microscopy

Scanning electron microscopy and fixing and staining of floral meristems were essentially performed as previously described (Fulton et al., 2009; Gao et al., 2019; Schneitz et al., 1997). Confocal laser scanning microscopy was performed with an Olympus FV1000 set-up using an inverted IX81 stand and FluoView software (FV10-ASW version 01.04.00.09, Olympus Europa) equipped with a water-corrected ×40 objective (NA 0.9) at ×3 digital zoom. For GFP fluorescence intensity measurements the mean gray values of GFP fluorescence signal intensity in the root epidermis of the pSUB::SUB:EGFP reporter was analyzed with ImageJ software (Schindelin et al., 2012). For each root, a region located 500 µm above the root tip (excluding the root cap) was used for analysis. To obtain the ratio between signal in cytoplasm versus total fluorescence intensity per cell we measured signal intensity in two different regions of interests (ROIs). One ROI covered the cytoplasm and the other ROI included the cytoplasm and the outer cell boundary.

For SUB:EGFP subcellular localization upon drug treatments or colocalization with FM4-64, confocal laser scanning microscopy was performed on epidermal cells of root meristems located ∼8-12 cells above the quiescent center using a Leica TCS SP8 X microscope equipped with GaAsP (HyD) detectors. The following objectives were used: a water-corrected ×63 objective (NA 1.2), a ×40 objective (NA 1.1), and a ×20 immersion objective (NA 0.75). Scan speed was set at 400 Hz, line average at between 2 and 4, and the digital zoom at 4.5 (colocalization with FM4-64), 3 (drug treatments) or 1 (root hair patterning). EGFP fluorescence excitation was performed at 488 nm using a multi-line argon laser (3% intensity) and detected at 502-536 nm. FM4-64 fluorescence was excited using a 561 nm laser (1% intensity) and detected at 610-672 nm. For the direct comparisons of fluorescence intensities, laser, pinhole and gain settings of the confocal microscope were kept identical when capturing the images from the seedlings of different treatments. For determination of colocalization, the distance from the center of each EGFP spot to the center of the nearest FM4-64 signal was measured by hand on single optical sections using ImageJ/Fiji software. If the distance between two puncta was below the resolution limit of the objective lens (0.24 µm) the signals were considered to colocalize (Ito et al., 2012). *Arabidopsis* seedlings were covered with a 22×22 mm glass coverslip of 0.17 mm thickness (no. 1.5H, Paul Marienfeld). Images were adjusted for color and contrast using ImageJ/Fiji software.

Steady state fluorescence anisotropy was measured using a FV3000 confocal laser scanning microscope (Olympus Europa) equipped with a single photon counting device with picosecond time resolution (LSM upgrade kit, PicoQuant). GFP was excited at 485 nm with a linearly polarized, pulsed (40 MHz) diode laser (LDH-D-C-485, PicoQuant) using a 60× water immersion objective (Olympus UPlanSApo, NA1.2). The emitted light was collected in the same objective and was separated into perpendicular and parallel polarization with respect to excitation polarization. GFP fluorescence was then detected using a PMA Hybrid 40 detector (PicoQuant) in a narrow range of its emission spectrum (BP520/35). A minimum 25 photons per pixel were counted with time correlated single photon counting (TCSPC) resolution of 25 ps of ROI size 512 px×512 px with 0.103 µM/px. Pixel-wise anisotropy was calculated with help of SymPhoTime 64 software (PicoQuant) using instrument correction factors L1 (0.035) and L2 (0.031) as well as the G-factor (1.018).

Statistics

Statistical analysis was performed with PRISM9 software (GraphPad Software). All statistical tests including *P*-values are described in the respective figure legends.

Acknowledgements

We acknowledge Ramon Torres Ruiz and other members of the Schneitz lab for helpful discussion and suggestions. We thank Ramon Torres Ruiz for help with the fluorescence anisotropy analysis, Herman Höfte for the *prc1-1* allele and the pTHE1::THE1:GFP line, Martin Stegmann for the pFER::FER:GFP line and Dolf Weijers for the TMO7:1×GFP and TMO7:3×GFP lines. We also thank Manfred Mayer for advice on statistics and Lynette Fulton for critical reading of the manuscript. We further acknowledge support by the Center for Advanced Light Microscopy (CALM) of the TUM School of Life Sciences.

Competing interests

The authors declare no competing or financial interests.

Author contributions

Conceptualization: A.C., X.C., S.W., K.S.; Methodology: A.C., X.C., B.L., R.B., J.G., S.W.; Formal analysis: A.C., X.C., B.L., R.B., S.W., K.S.; Investigation: A.C., X.C., B.L., R.B., J.G., S.W.; Writing - original draft: K.S.; Writing - review & editing: A.C., R.B., S.W., K.S.; Visualization: A.C., K.S.; Project administration: K.S.; Funding acquisition: S.W., K.S.

Funding

This work was funded by the German Research Council (Deutsche Forschungsgemeinschaft) through an Emmy Noether grant (WO 1660/2-2) to S.W. and an SFB924 grant (TP A2) to K.S.

Peer review history

The peer review history is available online at https://journals.biologists.com/dev/article-lookup/doi/10.1242/dev.199425

References

Bacete, L., Mélida, H., Miedes, E. and Molina, A. (2018). Plant cell wall-mediated immunity: cell wall changes trigger disease resistance responses. *Plant J.* **93**, 614-636. doi:10.1111/tpj.13807

Bader, A. N., Hoetzl, S., Hofman, E. G., Voortman, J., van Bergen en Henegouwen, P. M. P., van Meer, G. and Gerritsen, H. C. (2011). Homo-FRET imaging as a tool to quantify protein and lipid clustering. *Chemphyschem* **12**, 475-483. doi:10.1002/cphc.201000801

Baskin, T. I., Wilson, J. E., Cork, A. and Williamson, R. E. (1994). Morphology and microtubule organization in Arabidopsis roots exposed to oryzalin or taxol. *Plant Cell Physiol.* **35**, 935-942.

Berger, F., Taylor, A. and Brownlee, C. (1994). Cell fate determination by the cell wall in early *Fucus* development. *Science* **263**, 1421-1423. doi:10.1126/science.263.5152.1421

Box, M. S., Coustham, V., Dean, C. and Mylne, J. S. (2011). Protocol: a simple phenol-based method for 96-well extraction of high quality RNA from Arabidopsis. *Plant Methods* **7**, 7. doi:10.1186/1746-4811-7-7

Bringmann, M., Li, E., Sampathkumar, A., Kocabek, T., Hauser, M.-T. and Persson, S. (2012). POM-POM2/CELLULOSE SYNTHASE INTERACTING1 is essential for the functional association of cellulose synthase and microtubules in *Arabidopsis*. *Plant Cell* **24**, 163-177. doi:10.1105/tpc.111.093575

Chaudhary, A., Chen, X., Gao, J., Leśniewska, B., Hammerl, R., Dawid, C. and Schneitz, K. (2020). The Arabidopsis receptor kinase STRUBBELIG regulates the response to cellulose deficiency. *PLoS Genet.* **16**, e1008433. doi:10.1371/journal.pgen.1008433

Cheung, A. Y. and Wu, H.-M. (2011). THESEUS 1, FERONIA and relatives: a family of cell wall-sensing receptor kinases? *Curr. Opin. Plant Biol.* **14**, 632-641. doi:10.1016/j.pbi.2011.09.001

Chevalier, D., Batoux, M., Fulton, L., Pfister, K., Yadav, R. K., Schellenberg, M. and Schneitz, K. (2005). STRUBBELIG defines a receptor kinase-mediated signaling pathway regulating organ development in *Arabidopsis*. *Proc. Natl. Acad. Sci. USA* **102**, 9074-9079. doi:10.1073/pnas.0503526102

Chu, Z., Chen, H., Zhang, Y., Zhang, Z., Zheng, N., Yin, B., Yan, H., Zhu, L., Zhao, X., Yuan, M. et al. (2007). Knockout of the AtCESA2 gene affects microtubule orientation and causes abnormal cell expansion in Arabidopsis. *Plant Physiol.* **143**, 213-224. doi:10.1104/pp.106.088393

Cosgrove, D. J. (2018). Diffuse growth of plant cell walls. *Plant Physiol.* **176**, 16-27. doi:10.1104/pp.17.01541

Crowell, E. F., Bischoff, V., Desprez, T., Rolland, A., Stierhof, Y.-D., Schumacher, K., Gonneau, M., Höfte, H. and Vernhettes, S. (2009). Pausing of Golgi bodies on microtubules regulates secretion of cellulose synthase complexes in *Arabidopsis*. *Plant Cell* **21**, 1141-1154. doi:10.1105/tpc.108.065334

Desprez, T., Vernhettes, S., Fagard, M., Refrégier, G., Desnos, T., Aletti, E., Py, N., Pelletier, S. and Höfte, H. (2002). Resistance against herbicide isoxaben and cellulose deficiency caused by distinct mutations in same cellulose synthase isoform CESA6. *Plant Physiol.* **128**, 482-490. doi:10.1104/pp.010822

Desprez, T., Juraniec, M., Crowell, E. F., Jouy, H., Pochylova, Z., Parcy, F., Höfte, H., Gonneau, M. and Vernhettes, S. (2007). Organization of cellulose synthase complexes involved in primary cell wall synthesis in *Arabidopsis thaliana*. *Proc. Natl. Acad. Sci. USA* **104**, 15572-15577. doi:10.1073/pnas.0706569104

Du, J., Kirui, A., Huang, S., Wang, L., Barnes, W. J., Kiemle, S. N., Zheng, Y., Rui, Y., Ruan, M., Qi, S. et al. (2020). Mutations in the pectin methyltransferase QUASIMODO2 influence cellulose biosynthesis and wall integrity in Arabidopsis. *Plant Cell* **32**, 3576-3597. doi:10.1105/tpc.20.00252

Duan, Q., Kita, D., Li, C., Cheung, A. Y. and Wu, H.-M. (2010). FERONIA receptor-like kinase regulates RHO GTPase signaling of root hair development. *Proc. Natl. Acad. Sci. USA* **107**, 17821-17826. doi:10.1073/pnas.1005366107

Duckett, C. M., Grierson, C., Linstead, P., Schneider, K., Lawson, E., Dean, C., Poethig, S. and Roberts, K. (1994). Clonal relationships and cell patterning in the root epidermis of *Arabidopsis*. *Development* **120**, 2465-2474. doi:10.1242/dev.120.9.2465

Dünser, K., Gupta, S., Herger, A., Feraru, M. I., Ringli, C. and Kleine-Vehn, J. (2019). Extracellular matrix sensing by FERONIA and leucine-rich repeat extensins controls vacuolar expansion during cellular elongation in *Arabidopsis thaliana*. *EMBO J.* **38**, e100353. doi:10.15252/embj.2018100353

Echevin, E., Le Gloanec, C., Skowrońska, N., Routier-Kierzkowska, A.-L., Burian, A. and Kierzkowski, D. (2019). Growth and biomechanics of shoot organs. *J. Exp. Bot.* **70**, 3573-3585. doi:10.1093/jxb/erz205

Endler, A., Kesten, C., Schneider, R., Zhang, Y., Ivakov, A., Froehlich, A., Funke, N. and Persson, S. (2015). A mechanism for sustained cellulose synthesis during salt stress. *Cell* **162**, 1353-1364. doi:10.1016/j.cell.2015.08.028

Engelsdorf, T., Gigli-Bisceglia, N., Veerabagu, M., McKenna, J. F., Vaahtera, L., Augstein, F., Van der Does, D., Zipfel, C. and Hamann, T. (2018). The plant cell wall integrity maintenance and immune signaling systems cooperate to control stress responses in *Arabidopsis thaliana*. *Sci. Signal.* **11**, eaao3070. doi:10.1126/scisignal.aao3070

Enugutti, B., Kirchhelle, C., Oelschner, M., Torres Ruiz, R. A., Schliebner, I., Leister, D. and Schneitz, K. (2012). Regulation of planar growth by the *Arabidopsis* AGC protein kinase UNICORN. *Proc. Natl. Acad. Sci. USA* **109**, 15060-15065. doi:10.1073/pnas.1205089109

Fagard, M., Desnos, T., Desprez, T., Goubet, F., Refregier, G., Mouille, G., McCann, M., Rayon, C., Vernhettes, S. and Höfte, H. (2000). *PROCUSTE1* encodes a cellulose synthase required for normal cell elongation specifically in roots and dark-grown hypocotyls of Arabidopsis. *Plant Cell* **12**, 2409-2424. doi:10.1105/tpc.12.12.2409

Feng, W., Kita, D., Peaucelle, A., Cartwright, H. N., Doan, V., Duan, Q., Liu, M.-C., Maman, J., Steinhorst, L., Schmitz-Thom, I. et al. (2018). The FERONIA receptor kinase maintains cell-wall integrity during salt stress through Ca2+ signaling. *Curr. Biol.* **28**, 666-675.e5. doi:10.1016/j.cub.2018.01.023

Fisher, D. D. and Cyr, R. J. (1998). Extending the microtubule/microfibril paradigm: cellulose synthesis is required for normal cortical microtubule alignment in elongating cells. *Plant Physiol.* **116**, 1043-1051. doi:10.1104/pp.116.3.1043

Fulton, L., Batoux, M., Vaddepalli, P., Yadav, R. K., Busch, W., Andersen, S. U., Jeong, S., Lohmann, J. U. and Schneitz, K. (2009). *DETORQUEO*, *QUIRKY*, and *ZERZAUST* represent novel components involved in organ development mediated by the receptor-like kinase STRUBBELIG in *Arabidopsis thaliana*. *PLoS Genet.* **5**, e1000355. doi:10.1371/journal.pgen.1000355

Gao, J., Chaudhary, A., Vaddepalli, P., Nagel, M.-K., Isono, E. and Schneitz, K. (2019). The Arabidopsis receptor kinase STRUBBELIG undergoes clathrin-dependent endocytosis. *J. Exp. Bot.* **70**, 3881-3894. doi:10.1093/jxb/erz190

Gigli-Bisceglia, N., Engelsdorf, T., Strnad, M., Vaahtera, L., Khan, G. A., Jamoune, A., Alipanah, L., Novák, O., Persson, S., Hejatko, J. et al. (2018). Cell wall integrity modulates *Arabidopsis thaliana* cell cycle gene expression in a cytokinin- and nitrate reductase-dependent manner. *Development* **145**, dev166678. doi:10.1242/dev.166678

Gigli-Bisceglia, N., Engelsdorf, T. and Hamann, T. (2020). Plant cell wall integrity maintenance in model plants and crop species-relevant cell wall components and underlying guiding principles. *Cell. Mol. Life Sci.* **77**, 2049-2077. doi:10.1007/s00018-019-03388-8

Grossmann, G., Krebs, M., Maizel, A., Stahl, Y., Vermeer, J. E. M. and Ott, T. (2018). Green light for quantitative live-cell imaging in plants. *J. Cell Sci.* **131**, jcs209270. doi:10.1242/jcs.209270

Gu, Y., Kaplinsky, N., Bringmann, M., Cobb, A., Carroll, A., Sampathkumar, A., Baskin, T. I., Persson, S. and Somerville, C. R. (2010). Identification of a cellulose synthase-associated protein required for cellulose biosynthesis. *Proc Natl. Acad. Sci. USA* **107**, 12866-12871. doi:10.1073/pnas.1007092107

Gutierrez, R., Lindeboom, J. J., Paredez, A. R., Emons, A. M. C. and Ehrhardt, D. W. (2009). Arabidopsis cortical microtubules position cellulose synthase delivery to the plasma membrane and interact with cellulose synthase trafficking compartments. *Nat. Cell Biol.* **11**, 797-806. doi:10.1038/ncb1886

Hamann, T., Bennett, M., Mansfield, J. and Somerville, C. (2009). Identification of cell-wall stress as a hexose-dependent and osmosensitive regulator of plant responses. *Plant J.* **57**, 1015-1026. doi:10.1111/j.1365-313X.2008.03744.x

Heim, D. R., Roberts, J. L., Pike, P. D. and Larrinua, I. M. (1989). Mutation of a locus of *Arabidopsis thaliana* confers resistance to the herbicide isoxaben. *Plant Physiol.* **90**, 146-150. doi:10.1104/pp.90.1.146

Heim, D. R., Roberts, J. L., Pike, P. D. and Larrinua, I. M. (1990a). A second locus, Ixr B1 in *Arabidopsis thaliana*, that confers resistance to the herbicide isoxaben. *Plant Physiol.* **92**, 858-861. doi:10.1104/pp.92.3.858

Heim, D. R., Skomp, J. R., Tschabold, E. E. and Larrinua, I. M. (1990b). Isoxaben inhibits the synthesis of acid insoluble cell wall materials In *Arabidopsis thaliana*. *Plant Physiol.* **93**, 695-700. doi:10.1104/pp.93.2.695

Hématy, K., Sado, P.-E., Van Tuinen, A., Rochange, S., Desnos, T., Balzergue, S., Pelletier, S., Renou, J.-P. and Höfte, H. (2007). A receptor-like kinase mediates the response of Arabidopsis cells to the inhibition of cellulose synthesis. *Curr. Biol.* **17**, 922-931. doi:10.1016/j.cub.2007.05.018

Höfte, H. and Voxeur, A. (2017). Plant cell walls. *Curr. Biol.* **27**, R865-R870. doi:10.1016/j.cub.2017.05.025

Hynes, R. O. (2009). The extracellular matrix: not just pretty fibrils. *Science* **326**, 1216-1219. doi:10.1126/science.1176009

Ito, E., Fujimoto, M., Ebine, K., Uemura, T., Ueda, T. and Nakano, A. (2012). Dynamic behavior of clathrin in *Arabidopsis thaliana* unveiled by live imaging. *Plant J.* **69**, 204-216. doi:10.1111/j.1365-313X.2011.04782.x

Kesten, C., Wallmann, A., Schneider, R., McFarlane, H. E., Diehl, A., Khan, G. A., van Rossum, B.-J., Lampugnani, E. R., Szymanski, W. G., Cremer, N. et al. (2019). The companion of cellulose synthase 1 confers salt tolerance through a Tau-like mechanism in plants. *Nat. Commun.* **10**, 857. doi:10.1038/s41467-019-08780-3

Ketelaar, T., de Ruijter, N. C. A. and Emons, A. M. C. (2003). Unstable F-actin specifies the area and microtubule direction of cell expansion in Arabidopsis root hairs. *Plant Cell* **15**, 285-292. doi:10.1105/tpc.007039

Kwak, S.-H. and Schiefelbein, J. (2007). The role of the SCRAMBLED receptor-like kinase in patterning the *Arabidopsis* root epidermis. *Dev. Biol.* **302**, 118-131. doi:10.1016/j.ydbio.2006.09.009

Kwak, S.-H., Shen, R. and Schiefelbein, J. (2005). Positional signaling mediated by a receptor-like kinase in Arabidopsis. *Science* **307**, 1111-1113. doi:10.1126/science.1105373

Lampugnani, E. R., Khan, G. A., Somssich, M. and Persson, S. (2018). Building a plant cell wall at a glance. *J. Cell Sci.* **131**, jcs207373. doi:10.1242/jcs.207373

Lewis, K. C., Selzer, T., Shahar, C., Udi, Y., Tworowski, D. and Sagi, I. (2008). Inhibition of pectin methyl esterase activity by green tea catechins. *Phytochemistry* **69**, 2586-2592. doi:10.1016/j.phytochem.2008.08.012

Li, S., Lei, L., Somerville, C. R. and Gu, Y. (2012). Cellulose synthase interactive protein 1 (CSI1) links microtubules and cellulose synthase complexes. *Proc. Natl. Acad. Sci. USA* **109**, 185-190. doi:10.1073/pnas.1118560109

Lin, L., Zhong, S.-H., Cui, X.-F., Li, J. and He, Z.-H. (2012). Characterization of temperature-sensitive mutants reveals a role for receptor-like kinase SCRAMBLED/STRUBBELIG in coordinating cell proliferation and differentiation

during Arabidopsis leaf development. *Plant J.* **72**, 707-720. doi:10.1111/j.1365-313X.2012.05109.x

Liu, Z., Schneider, R., Kesten, C., Zhang, Y., Somssich, M., Zhang, Y., Fernie, A. R. and Persson, S. (2016). Cellulose-microtubule uncoupling proteins prevent lateral displacement of microtubules during cellulose synthesis in Arabidopsis. *Dev. Cell* **38**, 305-315. doi:10.1016/j.devcel.2016.06.032

Masucci, J. D., Rerie, W. G., Foreman, D. R., Zhang, M., Galway, M. E., Marks, M. D. and Schiefelbein, J. W. (1996). The homeobox gene *GLABRA2* is required for position-dependent cell differentiation in the root epidermis of *Arabidopsis thaliana*. *Development* **122**, 1253-1260. doi:10.1242/dev.122.4.1253

Paredez, A. R., Somerville, C. R. and Ehrhardt, D. W. (2006). Visualization of cellulose synthase demonstrates functional association with microtubules. *Science* **312**, 1491-1495. doi:10.1126/science.1126551

Paredez, A. R., Persson, S., Ehrhardt, D. W. and Somerville, C. R. (2008). Genetic evidence that cellulose synthase activity influences microtubule cortical array organization. *Plant Physiol.* **147**, 1723-1734. doi:10.1104/pp.108.120196

Persson, S., Paredez, A., Carroll, A., Palsdottir, H., Doblin, M., Poindexter, P., Khitrov, N., Auer, M. and Somerville, C. R. (2007). Genetic evidence for three unique components in primary cell-wall cellulose synthase complexes in Arabidopsis. *Proc. Natl. Acad. Sci. USA* **104**, 15566-15571. doi:10.1073/pnas.0706592104

Rui, Y. and Dinneny, J. R. (2020). A wall with integrity: surveillance and maintenance of the plant cell wall under stress. *New Phytol.* **225**, 1428-1439. doi:10.1111/nph.16166

Sampathkumar, A., Gutierrez, R., McFarlane, H. E., Bringmann, M., Lindeboom, J., Emons, A.-M., Samuels, L., Ketelaar, T., Ehrhardt, D. W. and Persson, S. (2013). Patterning and lifetime of plasma membrane-localized cellulose synthase is dependent on actin organization in Arabidopsis interphase cells. *Plant Physiol.* **162**, 675-688. doi:10.1104/pp.113.215277

Scheible, W.-R., Eshed, R., Richmond, T., Delmer, D. and Somerville, C. (2001). Modifications of cellulose synthase confer resistance to isoxaben and thiazolidinone herbicides in *Arabidopsis Ixr1* mutants. *Proc. Natl. Acad. Sci. USA* **98**, 10079-10084. doi:10.1073/pnas.191361598

Scheible, W.-R., Fry, B., Kochevenko, A., Schindelasch, D., Zimmerli, L., Somerville, S., Loria, R. and Somerville, C. R. (2003). An Arabidopsis mutant resistant to Thaxtomin A, a cellulose synthesis inhibitor from *Streptomyces* species. *Plant Cell* **15**, 1781-1794. doi:10.1105/tpc.013342

Schindelin, J., Arganda-Carreras, I., Frise, E., Kaynig, V., Longair, M., Pietzsch, T., Preibisch, S., Rueden, C., Saalfeld, S., Schmid, B. et al. (2012). Fiji: an open-source platform for biological-image analysis. *Nat. Meth.* **9**, 676-682. doi:10.1038/nmeth.2019

Schlereth, A., Möller, B., Liu, W., Kientz, M., Flipse, J., Rademacher, E. H., Schmid, M., Jürgens, G. and Weijers, D. (2010). MONOPTEROS controls embryonic root initiation by regulating a mobile transcription factor. *Nature* **464**, 913-916. doi:10.1038/nature08836

Schneitz, K., Hülskamp, M. and Pruitt, R. E. (1995). Wild-type ovule development in *Arabidopsis thaliana*: a light microscope study of cleared whole-mount tissue. *Plant J.* **7**, 731-749. doi:10.1046/j.1365-313X.1995.07050731.x

Schneitz, K., Hülskamp, M., Kopczak, S. D. and Pruitt, R. E. (1997). Dissection of sexual organ ontogenesis: a genetic analysis of ovule development in *Arabidopsis thaliana*. *Development* **124**, 1367-1376. doi:10.1242/dev.124.7.1367

Smyth, D. R., Bowman, J. L. and Meyerowitz, E. M. (1990). Early flower development in Arabidopsis. *Plant Cell* **2**, 755-767.

Somssich, M., Ma, Q., Weidtkamp-Peters, S., Stahl, Y., Felekyan, S., Bleckmann, A., Seidel, C. A. M. and Simon, R. (2015). Real-time dynamics of peptide ligand-dependent receptor complex formation in planta. *Sci. Signal.* **8**, ra76. doi:10.1126/scisignal.aab0598

Song, J. H., Kwak, S.-H., Nam, K. H., Schiefelbein, J. and Lee, M. M. (2019). QUIRKY regulates root epidermal cell patterning through stabilizing SCRAMBLED to control CAPRICE movement in Arabidopsis. *Nat. Commun.* **10**, 1744. doi:10.1038/s41467-019-09715-8

Stahl, Y., Grabowski, S., Bleckmann, A., Kühnemuth, R., Weidtkamp-Peters, S., Pinto, K. G., Kirschner, G. K., Schmid, J. B., Wink, R. H., Hülsewede, A. et al. (2013). Moderation of Arabidopsis root stemness by CLAVATA1 and ARABIDOPSIS CRINKLY4 receptor kinase complexes. *Curr. Biol.* **23**, 362-371. doi:10.1016/j.cub.2013.01.045

Staiger, C. J., Sheahan, M. B., Khurana, P., Wang, X., McCurdy, D. W. and Blanchoin, L. (2009). Actin filament dynamics are dominated by rapid growth and severing activity in the Arabidopsis cortical array. *J. Cell Biol.* **184**, 269-280. doi:10.1083/jcb.200806185

Tateno, M., Brabham, C. and DeBolt, S. (2016). Cellulose biosynthesis inhibitors - a multifunctional toolbox. *J. Exp. Bot.* **67**, 533-542. doi:10.1093/jxb/erv489

Trehin, C., Schrempp, S., Chauvet, A., Berne-Dedieu, A., Thierry, A.-M., Faure, J.-E., Negrutiu, I. and Morel, P. (2013). *QUIRKY* interacts with *STRUBBELIG* and *PAL OF QUIRKY* to regulate cell growth anisotropy during Arabidopsis gynoecium development. *Development* **140**, 4807-4817. doi:10.1242/dev.091868

Uyttewaal, M., Burian, A., Alim, K., Landrein, B., Borowska-Wykręt, D., Dedieu, A., Peaucelle, A., Ludynia, M., Traas, J., Boudaoud, A. et al. (2012). Mechanical stress acts via katanin to amplify differences in growth rate between adjacent cells in *Arabidopsis*. *Cell* **149**, 439-451. doi:10.1016/j.cell.2012.02.048

Vaahtera, L., Schulz, J. and Hamann, T. (2019). Cell wall integrity maintenance during plant development and interaction with the environment. *Nat. Plants* **5**, 924-932. doi:10.1038/s41477-019-0502-0

Vaddepalli, P., Fulton, L., Batoux, M., Yadav, R. K. and Schneitz, K. (2011). Structure-function analysis of STRUBBELIG, an Arabidopsis atypical receptor-like kinase involved in tissue morphogenesis. *PLoS ONE* **6**, e19730. doi:10.1371/journal.pone.0019730

Vaddepalli, P., Herrmann, A., Fulton, L., Oelschner, M., Hillmer, S., Stratil, T. F., Fastner, A., Hammes, U. Z., Ott, T., Robinson, D. G. et al. (2014). The C2-domain protein QUIRKY and the receptor-like kinase STRUBBELIG localize to plasmodesmata and mediate tissue morphogenesis in *Arabidopsis thaliana*. *Development* **141**, 4139-4148. doi:10.1242/dev.113878

Van der Does, D., Boutrot, F., Engelsdorf, T., Rhodes, J., McKenna, J. F., Vernhettes, S., Koevoets, I., Tintor, N., Veerabagu, M., Miedes, E. et al. (2017). The Arabidopsis leucine-rich repeat receptor kinase MIK2/LRR-KISS connects cell wall integrity sensing, root growth and response to abiotic and biotic stresses. *PLoS Genet.* **13**, e1006832. doi:10.1371/journal.pgen.1006832

Verbelen, J. P. and Kerstens, S. (2000). Polarization confocal microscopy and congo red fluorescence: a simple and rapid method to determine the mean cellulose fibril orientation in plants. *J. Microsc.* **198**, 101-107. doi:10.1046/j.1365-2818.2000.00691.x

Wang, S., Kurepa, J., Hashimoto, T. and Smalle, J. A. (2011). Salt stress-induced disassembly of Arabidopsis cortical microtubule arrays involves 26S proteasome-dependent degradation of SPIRAL1. *Plant Cell* **23**, 3412-3427. doi:10.1105/tpc.111.089920

Watt, F. M. and Fujiwara, H. (2011). Cell-extracellular matrix interactions in normal and diseased skin. *Cold Spring Harb. Perspect. Biol.* **3**, a005124. doi:10.1101/cshperspect.a005124

Weidtkamp-Peters, S. and Stahl, Y. (2017). The use of FRET/FLIM to study proteins Interacting with plant receptor kinases. *Methods Mol. Biol.* **1621**, 163-175. doi:10.1007/978-1-4939-7063-6_16

Whitewoods, C. D. and Coen, E. (2017). Growth and development of three-dimensional plant form. *Curr. Biol.* **27**, R910-R918. doi:10.1016/j.cub.2017.05.079

Xiao, C., Zhang, T., Zheng, Y., Cosgrove, D. J. and Anderson, C. T. (2016). Xyloglucan deficiency disrupts microtubule stability and cellulose biosynthesis in Arabidopsis, altering cell growth and morphogenesis. *Plant Physiol.* **170**, 234-249. doi:10.1104/pp.15.01395

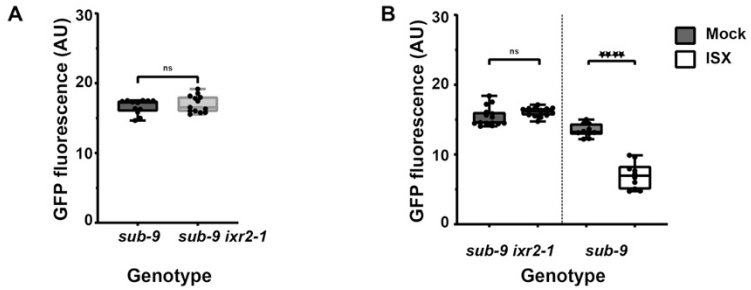

Fig. S1. Effect of isoxaben treatment on pSUB::SUB:EGFP expression. (A) Quantification of signal intensity of the pSUB::SUB:EGFP reporter in seven-day-old *sub-9* and *sub-9 i xr 2-1* plate-grown seedlings. Imaging parameters between both genotypes were identical. Box and whisker plots are shown. n ≤ 15. No statistical significance difference was observed (unpaired t-test with Welch's correction, two-tailed P values). The experiment was performed three times with similar results. (B) Quantification of signal intensity of the pSUB::SUB:EGFP reporter in seven-day-old plate-grown *sub-9* and *sub-9 i xr 2-1* seedlings transferred to plates containing 600 nM isoxaben for 8 hours. Imaging parameters between both genotypes were identical. Box and whisker plots are shown. 10 >n ≤ 15. No statistical significance difference was observed for treated or untreated sub-9 ixr2- 1 seedlings (****, P < 0.0001; one-way ANOVA followed by post hoc Tukey's multiple comparison test). The experiment was performed three times with similar results.

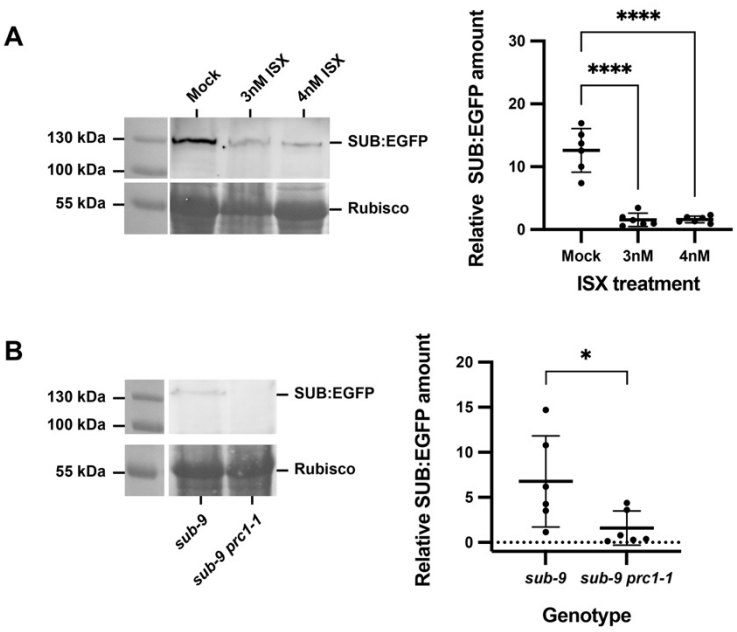

Fig. S2. Western blot analysis of pSUB::SUB:EGFP expression. (A) Left panel: Western blot depicting SUB:EGFP expression levels in seven-day-old plate-grown *sub-1* pSUB::SUB:EGFP seedlings exposed to mock or increasing amounts of isoxaben (ISX) using an anti-GFP antibody. The upper row shows the SUB:EGFP signal. The bottom row shows Ponceau staining depicting Rubisco bands as loading control. The experiment was performed twice with three biological replicates each. Right panel: quantification of signal intensity of all the biological replicates. SUB:EGFP signal intensity in each lane was normalized using the respective loading control. Mean +/- SD are indicated. Asterisks indicate statistical significance (****, $P < 0.0001$; one-way ANOVA followed by post hoc Tukey's multiple comparison test). (B) Western blot depicting SUB:EGFP expression levels in seven-day-old plate-grown *sub-9* pSUB::SUB:EGFP or *sub-9 prc1-1* pSUB::SUB:EGFP seedlings using an anti-GFP antibody. The upper row shows the SUB:EGFP signal. The bottom row shows Ponceau staining depicting Rubisco bands as loading control. The experiment was performed twice with three biological replicates each. Right panel: quantification of signal intensity of all the biological replicates. SUB:EGFP signal intensity in each lane was normalized using the respective loading control. Mean +/- SD are indicated. Asterisks indicate statistical significance (*, $P < 0.05$; two-tailed unpaired t test).

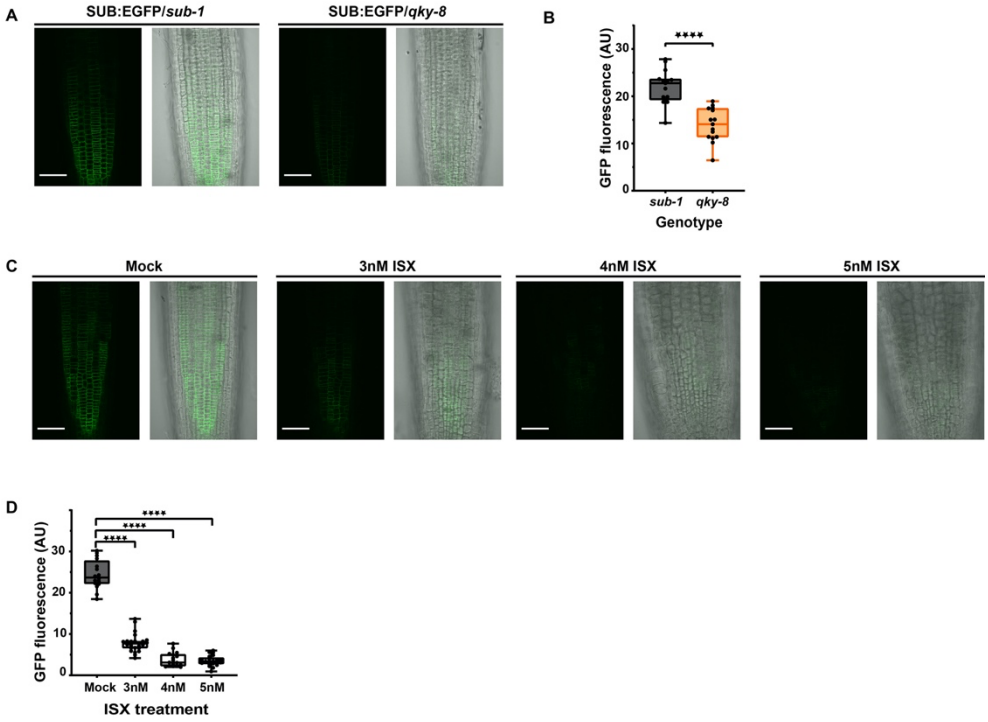

Fig. S3. Effect of isoxaben treatment on pSUB::SUB:EGFP expression pattern in *qky-8*. (A,C) show confocal micrographs depicting optical sections through roots of seven-day-old seedlings. (A) Signal intensity of a functional pSUB::SUB:EGFP reporter in *sub-1* and *qky-8* genetic background. Note the reduction of signal in *qky-8*. (B) Quantification of the data shown in (A). Box and whisker plots are shown. n =15. Asterisks represent statistical significance (****, $P < 0.0001$; unpaired t-test with Welch's correction, two-tailed P values). The experiment was performed three times with similar results. (C) Signal intensity of a functional pSUB::SUB:EGFP reporter in *qky-8*. Continuous treatments are indicated. Duration of treatment and treatment are indicated. Imaging parameters between mock and isoxaben treatments were identical. Note the reduced signal in isoxaben-treated seedlings. (D) Quantification of the data shown in (C). Box and whisker plots are shown. $16 \leq n \leq 25$. Asterisks represent statistical significance (****, $P < 0.0001$; one-way ANOVA followed by post hoc Tukey's multiple comparison test). The experiment was performed three times with similar results. Scale bars: 50 µm.

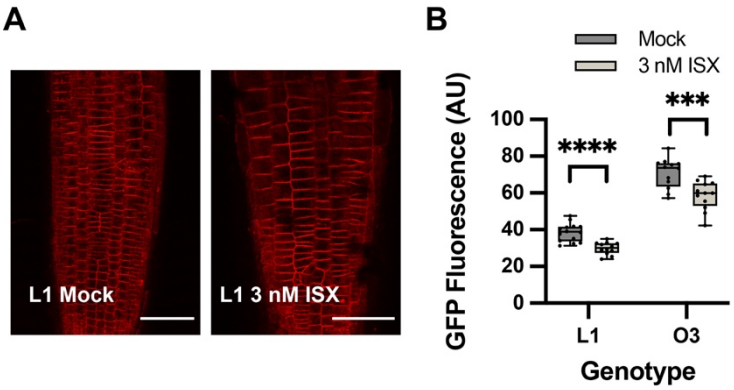

Fig. S4. Effect of isoxaben treatment on SUB:mCherry overexpression. The two independent Col lines homozygous for the pUBQ::SUB:mCherry construct (L1, O3) also carry the pGL2::GUS:EGFP reporter. Genotype and treatment are indicated. (A) Representative confocal micrographs depicting SUB:mCherry signal in optical sections through roots of seven-day-old L1 seedlings grown for five days on regular MS plates followed by exposure to mock or 3 nM isoxaben for 48 hours. Imaging parameters between mock and isoxaben treated seedlings were identical. (B) Quantification of the data shown in (A). Box and whisker plots encompassing all data points are shown. 12 ≤ n ≤ 14. In both lines a small but statistically significant decrease in signal intensity was observed upon exposure to isoxaben (****, P < 0.0001; ***, P < 0.002; unpaired t tests with Welch correction). The experiment was performed twice with similar results. Scale bars: 50 µm.

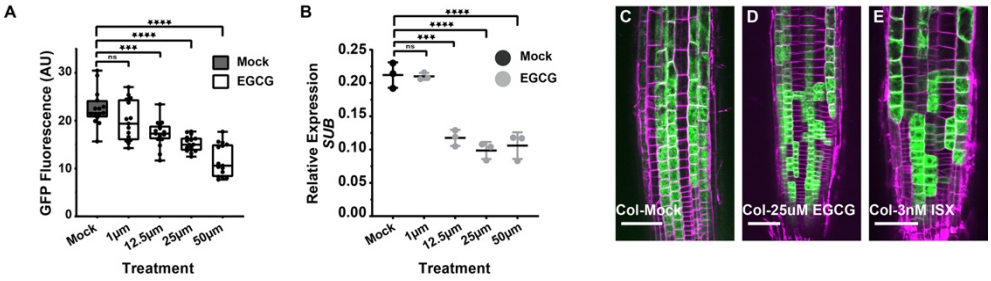

Fig. S5. Effects of EGCG treatment on pSUB::SUB:EGFP, *SUB* and pGL2::GUS:EGFP expression patterns. (A) Box and whisker plot shows quantification of signal intensity of the pSUB::SUB:EGFP reporter upon continuous exposure of plate-grown seedlings to mock or to indicated amount of EGCG treatment (n=15). Asterisks represent statistical significance (***, P < 0.0006; ****, P < 0.0001; one-way ANOVA followed by post hoc Tukey's multiple comparison test). The experiment was performed three times with similar results. (B) Relative transcript levels of *SUB* in seven-days-old seedlings exposed to mock or EGCG for indicated amount and time. Expression was detected by qPCR. Mean ± SD is shown, n=3. Asterisks represent statistical significance (***, P < 0.0006; ****, P < 0.0001; one-way ANOVA followed by post hoc Tukey's multiple comparison test). The experiment was performed three times with similar results. (C-E) confocal micrographs depicting optical sections through roots of seven-day-old seedlings showing the pGL2::GUS:EGFP expression pattern. Genotypes and/or treatments are indicated. 10/10 (C), 13/15, (D) 11/14 (E) root analyzed showed this pattern. Scale bars: 50 µm.

Supplementary Materials and Methods

Plant genetics

To generate the *sub-9 ixr2-1* double mutant F2 progeny of a parental cross between *sub-9* and *ixr2-1* were genotyped to select the double mutants. To generate the *pSUB::SUB:EGFP sub-9 ixr2-1* and *pSUB::SUB:EGFP sub-9 prc1-1* lines, the previously reported pSUB::SUB:EGFP plasmid was transformed into *sub-9*. Homozygous complementing T3 *pSUB::SUB:EGFP sub-9* was crossed into *sub-9 prc1-1* and *sub-9 ixr2-1* double mutants, respectively, and the F2 progeny was screened for double mutants with pSUB::SUB:EGFP expression and further propagated to obtain homozygous F3 lines. The *sub-9* pGL2::GUS:EGFP and *prc1-1* pGL2::GUS:EGFP lines were obtained by crossing the reporter line pGL2::GUS:EGFP into *sub-9* and *prc1-1*.

Table S1. Primers used in this study

Primer name	Sequence
R1(at4g33380) LP	5'- TGAAGGAGAGGAAGAGCCTGAGGAA -3'
R1(at4g33380) RP	5'-CCCCATCTCACTGCAGCACCAC -3'
R2 At2g28390 LP	5'-AGATTGCAGGGTACGCCTTGAGG-3'
R2 At2g28390 RP	5'- ACACGCATTCCACCTTCCGCG -3'
R3 At5g46630 LP	5'- CCAAATGGAATTTCAGGTGCCAATG -3'
R3 At5g46630 RP	5'- CAATGCGTACCTTGAGAAAACGAAC-'3
SUB(AT1G11130) LP	5'- GTTTGGATCTTTGACCTAGACGA-3'
SUB(AT1G11130) RP	5'- CAAGTTATTAATCGCCGAAACAT-3'